EADS INNOVATION WORKS

International Committee on Aeronautical Fatigue 2009

Review of Aeronautical Fatigue Investigations in Germany during the Period 2007 to 2009

Dr. Claudio Dalle Donne
Pascal Vermeer
EADS Innovation Works
CTO/IW-MS-2009-076

EADS

Title

Review of Aeronautical Fatigue Investigations in Germany during the Period May 2007 to April 2009

Author
Dr. Claudio Dalle Donne
Pascal Vermeer

Project-No.

Phone	Department/Work area	Date	Report-Nr.
+49-89.607 27728	CTO/IW-MS	June 2009	CTO/IW-MS-2009-076

Abstract

Within the scope of the 2009 Meeting of the International Committee on Aeronautical Fatigue in Rotterdam, this review embodies a compilation of abstracts on aeronautical fatigue investigations in Germany during the period May 2007 to April 2009.

The contribution of summaries by German aerospace manufacturers, governmental and private research institutes, universities as well as aerospace authorities was completely voluntary, and is acknowledged with sincere appreciation by the authors of this review.

Enquiries concerning the contents should be addressed directly to the author of the corresponding summary.

Distribution to

CTO/IW-GS-Patents (e-mail to Mrs. Rotter)
M&W Zander / KD – Dokumentenverarbeitung/Mikrofilm
Coverpage: CTO/IW – Yann Barbaux, CTO/IW-MG – Mr. Lindemann (via e-mail in pdf. format)

pages	photos	drawings	diagrams	tables
61				

Keywords for database

International Committee on Aeronautical Fatigue, ICAF 2009, National Delegate Review

[1] Classification

1 generally accessible
2 free distribution inside EADS
3 confidential
4 highly confidential

Acceptance

Dr. Claudio Dalle Donne
Head of responsible department

Table of contents

1 Introduction 7
2 Full Scale Testing 8
2.1 Overview of Full Scale Fatigue Tests (May 2009) 8
2.2 A380 Full Scale Fatigue Test – News Flash 2008 8
2.3 Airbus A320 Fatigue Testing for an Extended Service Goal 9
2.4 Design and Testing of Innovative Flap Support Structures 10
2.5 Spherical Bearing Test 12
2.6 Engine Structure Fatigue Test 13
2.7 Rudder Fittings Component Tests 13
2.8 Fatigue Test of a Tay LP Shaft Assembly 14
2.9 Rolls-Royce BR725 - Rear Mount Ring Static and Fatigue Tests 15
2.10 Fatigue Test of the Tornado NLG Backup Structure 16
3 Fatigue and Fracture of Fuselage Panels and Joints 18
3.1 Fatigue Crack Growth in FSW Joints Subjected to In-phase Biaxial Loads 18
3.2 Improvement of Damage Tolerance of Laser Beam Welded Aluminum Panels via Crenellations 20
3.3 Experimental Investigation on Bonded Structures for increased Damage Tolerant Aircraft Structures 21
3.4 The Effect of Bonded Doublers on Fatigue Crack Initiation/Propagation in Longitudinal FSW Joints in Fuselage Panels 23
3.5 Bonded Repair for Fuselage Damage: an Overall Benefit to Commercial Aviation 26
3.6 Hybrid Structure Solution for the A400m Wing Attachment Frames 27
3.7 Dialfast - Curved Fuselage Panel Fatigue and Damage Tolerance Test 28
3.8 Performance of Fatigue Crack Initiation and Propagation Tests for Supporting Assessment of Repair Solutions in Riveted Glare Joints 29
4 Fatigue Life Assessment and Prediction 31
4.1 General Reliability Theory in Elastic Mathematics 31
4.2 General Risk Theory in Elastic Mathematics 32
5 Fatigue and Fracture of Metallic Fuselage Materials 34
5.1 Crack Detection using a Contact-Free Optical Measurement Method 34
5.2 Laser Shock Peening to Improve the Fatigue Resistance of Highly Stressed Structural Components 36
5.3 Linear Combination Method in Three-Dimensional Elasticity 38
5.4 Analytic Macroelement Method in Axially Symmetric Elasticity 39
6 Fatigue and Fracture of Composites 41
6.1 Damage Behaviour of Hybrid Titanium-PEEK /AS4 Composite Laminates in Mixed Mode Bending – Experiments and Numerical Simulations 41
6.2 Hybrid Structures for Concentrated Load Transmission in Fibre Composites: Initial Experiments 43
6.3 Fatigue Crack Growth in CFRP Foam-Core Sandwich Structures 45
6.4 With a “Plastic Balloon” Through the Mars Atmosphere 47
6.5 Next Generation of Composites Structures Sizing Criteria 51
6.6 Generalization of the Tresca Criterion in General Strength Theory 52
6.7 Generalization of the Huber-von-Mises-Henky Criterion in General Strength Theory 54
7 Fatigue and Fracture of Engine Materials 56
7.1 Fatigue Strength Reduction of TiAl-Alloys by Impact Damage 56
8 Non-Destructive Testing and Structural Health Monitoring 57
8.1 Influence of Cyclic Loading and Temperature on Integrity of Piezoceramic Patch Transducers 57

8.2 Corrections and Generalizations of the Least Square Method 59
8.3 General Theory of Measuring Inhomogeneous Distributions 60

Tables

Table 2.1: Overview of full scale tests, currently running and/or finalised between 2007 and 2009 8

Figures

Figure 2.1 Double-shot view of the A380EF wing deflection during fatigue cycling 9
Figure 2.2 A320 ESG centre fuselage with wings (NEF2) and rear fuselage (NEF3) 10
Figure 2.3: Normal view including the template column 11
Figure 2.4: Test article up-side down in test rig 11
Figure 2.5 Spherical bearing 12
Figure 2.6 Test rig 12
Figure 2.7 Dummy casings 13
Figure 2.8 Test rig 13
Figure 2.9 Rudder fitting 14
Figure 2.10 MTA with the non-rotating LP shaft and hydraulic actuators 15
Figure 2.11 Test Set-up of the BR725 Rear Mount Ring test 16
Figure 2.12 Set-up of Nose Landing Gear Test 17
Figure 3.1 Cruciform specimen 19
Figure 3.2 Crack growth for butt joint and stringer specimens loaded biaxially as indicated (starter notch parallel to the weld seam) 19
Figure 3.3 Crack starter and crack initiation at the starter notch as observed on specimen back side for loading conditions as indicated 19
Figure 3.4 da/dn-$\triangle$K curves calculated according to Leevers et al. [3], reference data from uniaxially loaded base material 19
Figure 3.5 Mode I stress intensity factor (K_I) profile for a centre crack on a 740 mm wide aluminium panel with five laser beam welded stringers. Values were normalized with the values for a smooth reference panel of equal outer dimensions and weight 20
Figure 3.6 Crack length vs. number of fatigue cycles diagram for reference and crenellated panels tested under modified mini-TWIST spectrum showing the substantial fatigue life improvement due to crenellations 21
Figure 3.7 Test coupon: “seven stringers” panel with (a) doublers bonded between and below the stringers, with (b) additional glass fibre reinforcement 22
Figure 3.8 Effect of aluminum bonded doubler in the middle of the stringer bay 23
Figure 3.9 Schematic representation of the FSW panels 24
Figure 3.10 S-N curve for FSW panels comparing bonded doubler geometry 25
Figure 3.11 Left: $\triangle$K*–da/dN curve for FSW panels and Airbus reference (AIMS). $\triangle$K* with doubler correction (open markers). Right: 2a-N curve for FSW panels until failure, calculated stress correction for panel 3. 25
Figure 3.12 The A400M fuselage with the centre section and the division of the centre section 27
Figure 3.13 IMA Test-rig V0 29
Figure 3.14 Flap after residual strength testing 29
Figure 3.15 Riveted GLARE longitudinal joint specimen with integrated vacuum foil sensors .. 30
Figure 5.1 Displacement Field of a damaged CCT-specimen 35
Figure 5.2 Different methods for placing high-contrast spots on the specimen surface 35
Figure 5.3 Sketch and photograph of Laser shock peening process at MIC 36

Figure 5.4 Fatigue test results of anodized, milled, shot peened and laser shock peened notched specimens..... 37
Figure 5.5 Residual stress profile of shot peened and laser shock peened fatigue specimens. 37
Figure 6.1 MMB test apparatus and schematic loading description after [1]..... 41
Figure 6.2 Comparison between simulation and experiment of MMB test for a) UD-laminates with different mode mixtures and b) different MD lay ups for 50% mode mixture 42
Figure 6.3 Schematic lay-up of a hybrid laminate with its corresponding areas HTCL (2×Ti / 3×CFRP) with hole, Transition zone and CFRP (0°/90°)..... 43
Figure 6.4 Actual stresses in metal and fibre layers due to curing and additional applied stresses. Intersection at 411MPa 44
Figure 6.5 HTCL–2/3 fatigue crack propagation specimen. 44
Figure 6.6 Modified DCB-Test..... 45
Figure 6.7 Modified ENF-Test 45
Figure 6.8 Load-Displacement-Curve quasi-static DCB-Test 46
Figure 6.9 Crack growth diagram 46
Figure 6.10 Demonstration of the ARCHIMEDES-balloon during the flight through the outer mars atmosphere..... 49
Figure 6.11 Chemical structures of the two polymers Upilex RN and PBO 49
Figure 6.12 Thermo gravimetric behaviour of Upilex RN and PBO..... 49
Figure 6.13 Dynamic-mechanical behaviour of Upilex RN and PBO. 50
Figure 6.14 Loss coefficient tan δ of Upilex RN and PBO..... 50
Figure 6.15 Static TCT Critical Energy Release Rate Data (Mode II) 51
Figure 6.16 Definition of the J- Integral and its applicability in StressCheck® 52
Figure 7.1 Front side damage of an edge impacted specimen before fatigue testing..... 56
Figure 7.2 Back side crack network of the same edge impacted specimen before fatigue testing. 56
Figure 8.1 Loading principle and setup of 4-point-bending test (here: a) PZT patch under tensile loading, b) patch on CRFP specimen)..... 57
Figure 8.2 Fatigue life diagram for mechanical tensile loading of PZT patches at different temperatures. Insertion: typical damage pattern (cracks in PZT)..... 58

1 Introduction

Within the scope of the 2009 Meeting of the International Committee on Aeronautical Fatigue in Rotterdam, this review embodies a compilation of abstracts on aeronautical fatigue investigations in Germany during the period May 2007 to April 2009.
The contribution of summaries by German aerospace manufacturers, governmental and private research institutes, universities as well as aerospace authorities was completely voluntary, and is acknowledged with sincere appreciation by the authors of this review.
Enquiries concerning the contents should be addressed directly to the author of the corresponding summary.

Mailing addresses of contributing companies and institutes:

Abbreviation	Details
Airbus-D	Airbus Deutschland GmbH, Kreetslag 10, 21129 Hamburg, www.airbus.com
ALCAN CRV	Alcan Centre de Recherches de Voreppe, 725, rue Aristide Berges, Voreppe, 38341, France
EADS-IW	European Aeronautic Defence and Space Company, Innovation Works, 81663 Munich, www.eads.net
DLR	German Aerospace Center DLR, Institute of Materials Research, 51170 Cologne, www.dlr.de
GKSS	GKSS Research Centre, Max-Planck-Straße 1, 21502 Geesthacht, www.gkss.de
HAW	Hamburg University of Applied Science, Berliner Tor 5, 20099 Hamburg, www.haw-hamburg.de
IABG	Industrieanlagen-Betriebsgesellschaft mbH, PO-Box 1212, 85503 Ottobrunn, www.iabg.de
IFST	Academic Institute for Fundamental Scientific Theories, Augustenstraße 28, 80333 Munich
IMA	Materialforschung und Anwendungstechnik GmbH, PO-Box 800144, 01101 Dresden, www.ima-dresden.de
Fraunhofer	Fraunhofer Institut for Mechanics of Materials, Walter-Hülse-Strasse 1, 06120 Halle, www.iwm.fraunhofer.de
Premium Aerotec	Premium AEROTEC GmbH, Rechliner Straße, 85077 Manching, www.premium-aerotec.com
Shell	Shell Chemicals Europe, Engineering Integrity Department, Badhuisweg 3, 1031 CM Amsterdam, Netherlands, www.shell.com
TU Delft	Delft Universtity of Technology, Faculty of Aerospace Engineering, Group Aerospace Materials, Kluyverweg 1, 2629 HS Delft, Netherlands www.vm.lr.tudelft.nl
TUD-AI	Delft Universtity of Technology, Faculty of Aerospace Engineering, Adhesion Institute, Kluyverweg 1, 2629 HS Delft, Netherlands www.hechtingsinstituut.nl
Uni-Bologna	University di Bologna, www.eng.unibo.it
UniBw-M	University of the Federal Armed Forces Munich, Department of Materials Science, 85577 Neubiberg, www.unibw.de
Uni-Paderborn	University of Paderborn, Warburger Straße 100, 33098 Paderborn, www.uni-paderborn.de

2 Full Scale Testing

2.1 Overview of Full Scale Fatigue Tests (May 2009)

Project	Customer	Test Structure	Schedule	Laboratory
DIALFAST	Airbus-D	Curved panel fatigue and damage tolerance test	2003 - 2007	IMA
A300	Airbus-F	Curved panel test	2008	IMA
M-346	Liebherr	Nose landing gear test - NLG stiffness, strength and fatigue test 5th life	2009	IMA
A400M	Airbus-F	Rudder fittings component test	2008 - 2009	IMA
A380	Airbus-F	Pylon rod fatigue test	2008	IMA
A400M	TEI	Front bearing support test	2008 - 2009	IMA
A380	Airbus-D	A380 Full scale fatigue test	2003 - …	IABG
A320 NEF2	Airbus	A320 ESG NEF2 Full-scale fatigue test	2007 - 2011	IABG
A320 NEF3	Airbus	A320 ESG NEF3 Full-scale fatigue test	2007 - 2011	IABG
BR725 Engine	Rolls-Royce	Static and fatigue tests of rear mount ring	2007 - 2009	IABG
Tay Engine	Rolls-Royce	Fatigue test of a Tay LP shaft assembly	2007 - 2008	IABG
Tornado	EADS	Fatigue test of NLG backup structure	2003 - 2010	IABG
(A380)	Airbus	Fatigue crack initiation and propagation tests of riveted GLARE joints	2008 - 2009	IABG

Table 2.1: Overview of full scale tests, currently running and/or finalised between 2007 and 2009

2.2 A380 Full Scale Fatigue Test – News Flash 2008

F. Eichelbaum (IABG)

IABG continued the A380 full scale fatigue test in its Dresden site throughout the years 2007 and 2008. Meanwhile two times the A380EF design service goal has been successfully tested and more than 50 special measurement campaigns have been accomplished.
The aircraft symmetry is used by Airbus to simultaneously test the A380 serial production standard (right hand side) and to introduce new structural technologies or repair solutions for validation (left hand side).
IABG provided the mechanical test set-up in terms of test rig and loading trees, as well as the hydraulic actuators, the control & monitoring system and data acquisition system. Responsibility is held for operating the test and for conducting the regular aircraft structures inspections, including the documentation of inspection results.
The test will continue for another half of the A380 design service goal.

Figure 2.1 Double-shot view of the A380EF wing deflection during fatigue cycling

2.3 Airbus A320 Fatigue Testing for an Extended Service Goal

G. Hilfer, N. Rößler and C. Peters (IABG)

Within the scope of the Extended Service Goal (ESG) for the A320 family, fatigue tests (NEF) have been issued by Airbus in order to support analysis and justification for an extension of the limit of validity (LoV) of the maintenance program to ensure continuation of safe aircraft operation. A320/A321 major fatigue tests are developed by Airbus as supporting test basis for the analytical development of fatigue and damage tolerance justification up to 60.000 operational flight cycles (120.000 flight hours) as prime objective and up to 90.000 operational flight cycles (180.000 flight hours) as target objective for an extended LoV. The test aims will be achieved by 'Multiple Sections' testing, which divides the aircraft into three major test specimens: NEF1 representing the forward fuselage, NEF 2 representing the centre fuselage and wings and NEF3 representing the rear fuselage. For all three tests up to 180.000 SF have to be performed to simulate the fatigue and damage tolerance behaviour of the airframe. As with previous aircraft, Airbus again cooperates with IABG, appointed as responsible test institute for NEF2 and NEF3.

The concepts of the new fatigue tests have been developed based on the experience and cognitions of former tests for Airbus, in particular the A320 EF tests approximately 20 years ago when EF2 was accomplished by IABG and EF3 by Airbus Hamburg. Nevertheless, since the new tests have been taken into Airbus` program at very short notice, the realisation of the test

set-up required unique and very time efficient solutions in all needs. Due to this tight scheduling the implementation of NEF2 and NEF3 is incomparable to all previous aircraft tests for Airbus and one of its kind – although many components or at least the ideas of the set-up have been adopted from previous tests.

The application of established technologies and structures does not only save time, but also reduces the potential risk of faults caused by the use of non-field-tested technologies and structures. Some innovations, however, have been implemented to the new A320 fatigue tests like the concept of a pressurized fuselage without any volume reduction provisions and improvements of the layout capabilities of load introduction pad groups which no longer have to observe the requirement of a rectangular arrangement.

These tests have been taken into operation in early and late summer 2008. The testing speed is factor 2.1 higher than for the previous A320 test. Both tests are progressing at a fast rate and are according to plan.

A detailed presentation of these tests is given in a dedicated paper presented during the ICAF Symposium 2009.

Figure 2.2 A320 ESG centre fuselage with wings (NEF2) and rear fuselage (NEF3)

2.4 Design and Testing of Innovative Flap Support Structures

T. Havar (EADS IW) and E. Stuible (Premium Aerotec)

Innovative composite structures are increasingly being used in the aircraft industry. A critical point of these composite parts is their attachment to the surrounding aircraft structure. In cooperation between different EADS Business Units, a new advanced composite flap support system is developed to minimize weight and manufacturing costs (Figure 2.3). It consists of a hybrid flap track functioning as load carrying fairing (composite skin) with an aluminium frame and an innovative composite kinematics system. The kinematics system has several composite linkages and fittings, which connect the flap to the flap track. The linkages with two attachment points are primarily exposed to tension and compression loads. Therefore, these linkages are designed as load introduction loops. Linkages with three attachments points and fittings typically carry multiple loadings and are consequently designed as composite lugs. Each linkage element is analyzed using non linear finite element methods showing sufficient strength for the occurring loads.

Innovative manufacturing concepts for the composite linkages and the flap track are developed to minimize manufacturing costs. The complete composite flap support system is manufactured and verified on a prototype level.

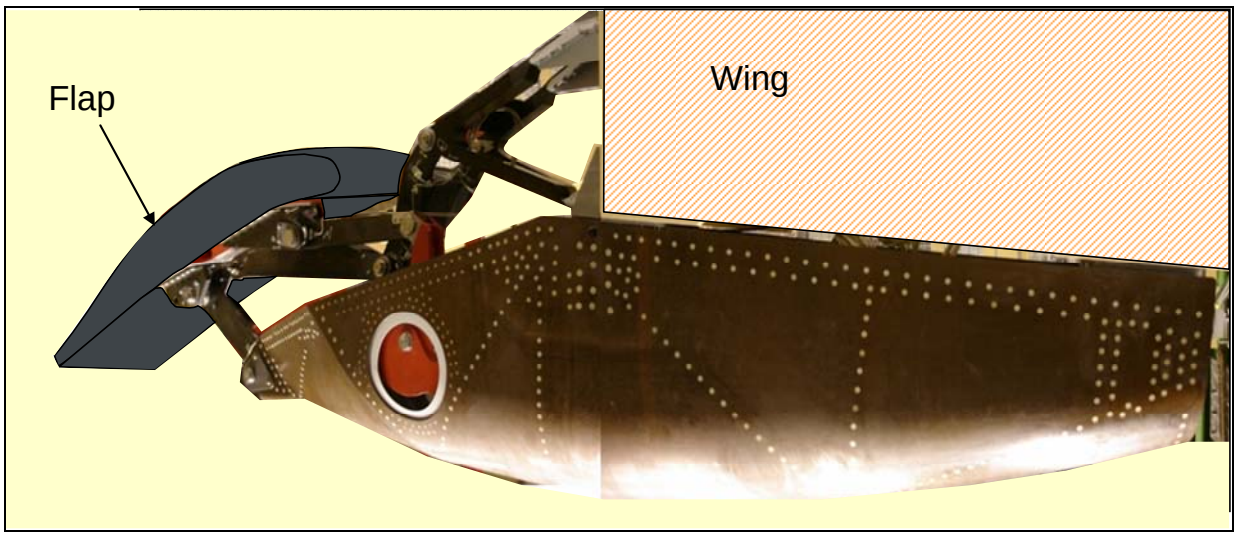

Figure 2.3: Normal view including the template column

The flap support system is validated with a full scale fatigue test (Figure 2.4) in accordance with Airbus specifications. The fatigue test proved that the composite flap support system is able to withstand all fatigue as well as static loads even with predefined defects.

Figure 2.4: Test article up-side down in test rig.

2.5 Spherical Bearing Test

D. Melzer (IMA)

IMA GmbH Dresden performed a fatigue test on a spherical bearing for NMB Minebea UK Ltd., Figure 2.5. The test program was realised describing the effects of bearing friction and bearing wear as a result of

- different loads in radial and axial direction
- simultaneous displacement (rotational and tilt) of the inner and outer bearing ring

Loads and displacements were combined in three different profiles. The bearing was tested for 120,000 cycles in complete. The test rig is shown in Figure 2.6.

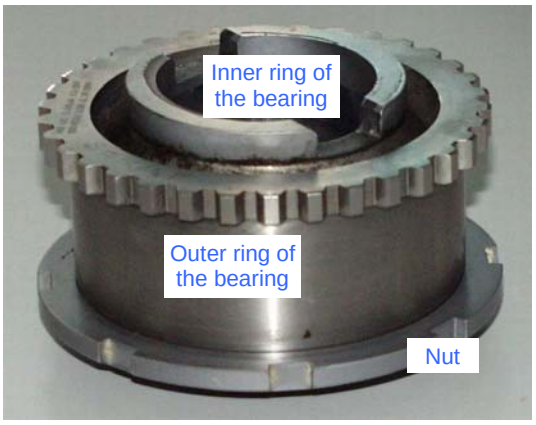

Figure 2.5 Spherical bearing

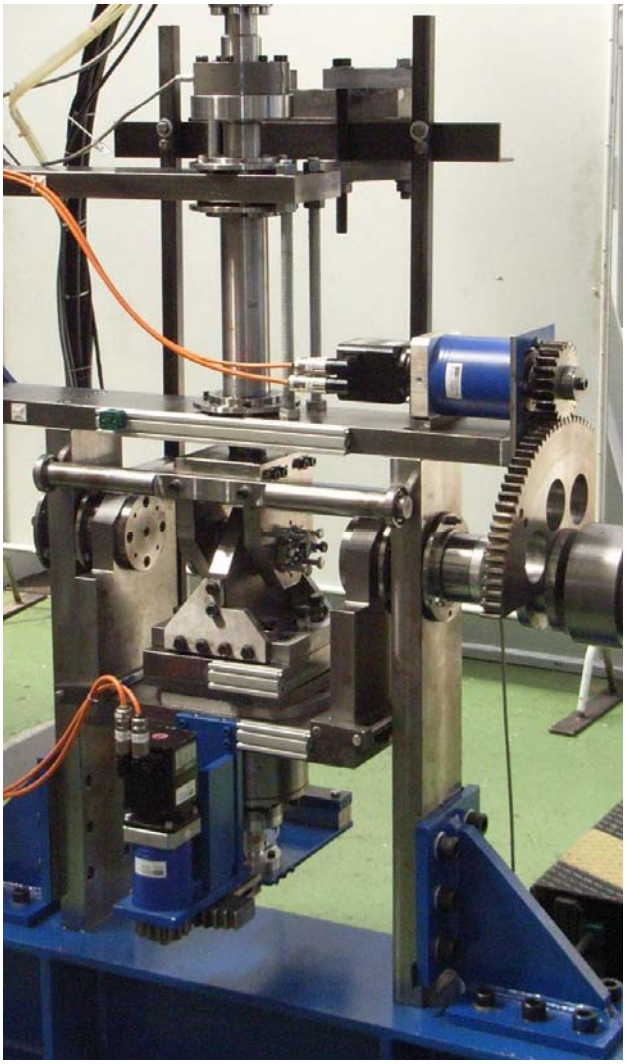

Figure 2.6 Test rig

2.6 Engine Structure Fatigue Test

M. Sachse (IMA)

IMA GmbH Dresden performed a fatigue test on a titanium aero engine casing. Due to the required force flows within the casing, special dummy structures were designed for loading the specimen. The challenge was to have the steel dummies meet the stiffness of the adjoining titanium casings within the engine.

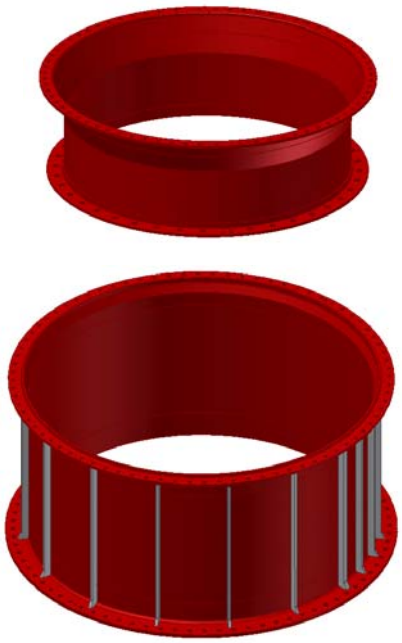

Figure 2.7 Dummy casings

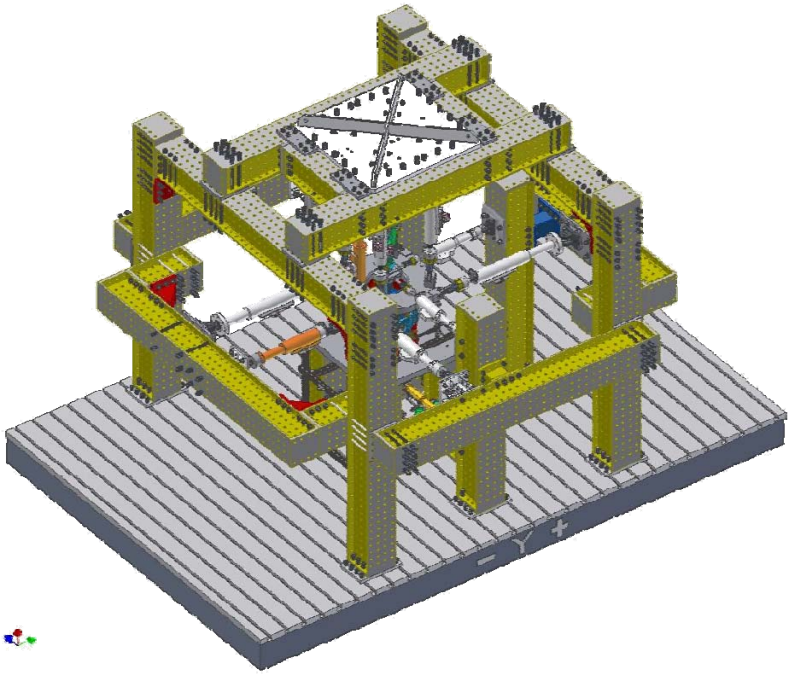

Figure 2.8 Test rig

19 hydraulic actuators were used for loading the structure. The test program consisted of 100.000 simulated flights, in which the specimen was monitored by strain gauges, LVDTs and by NDI. No damage was found after completion of the test program.

2.7 Rudder Fittings Component Tests

F. Wießner (IMA)

IMA GmbH Dresden performed a fatigue test of airplane rudder attachment fittings for Airbus France. Two different types of specimens have been tested to verify the fatigue calculations. The complex loading fatigue spectrum was defined by loads on three actuator lugs. Fittings (Figure 2.9) were loaded in fixed directions. For each specimen three actuators were used.
The specimens were tested for 50.000 cycles. Regular visual and NDT-inspections were performed during the fatigue test, after which no damage was detected.
Data signals of applied loads, displacements and S/G's were captured during the tests. At the end of the program, each specimen was subjected to a limit load test.

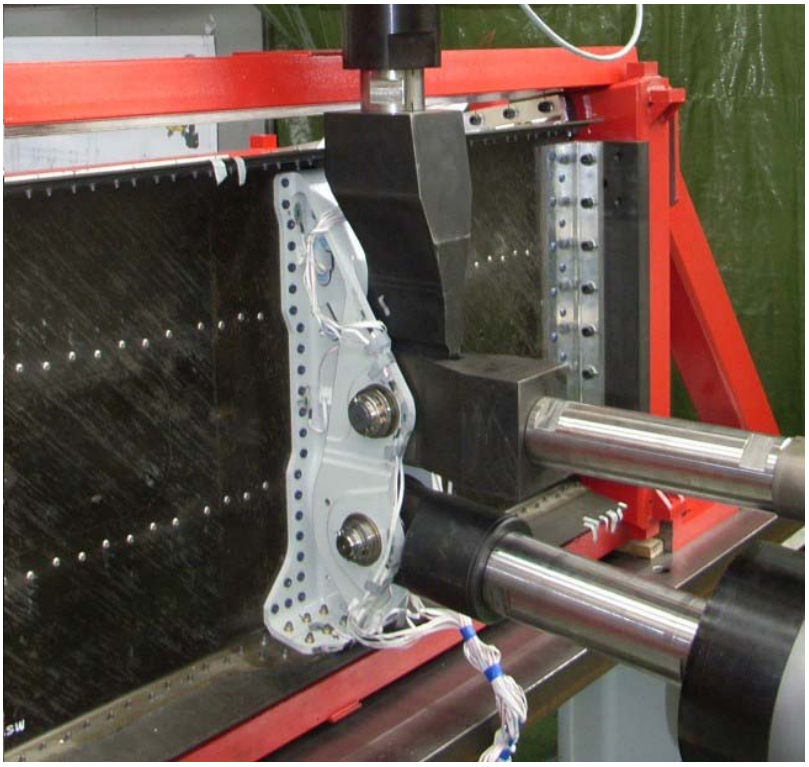

Figure 2.9 Rudder fitting

2.8 Fatigue Test of a Tay LP Shaft Assembly

W. Abrecht and G. Hilfer (IABG)

In the time frame September 2007 to February 2008, IABG tested a Rolls-Royce low pressure shaft assembly of the Tay engine.

This Tay LP shaft assembly – consisting mainly of the compressor shaft, the intermediate shaft and the turbine shaft – needed to be qualified for new life requirements. The loads on the shaft arrangement during operation were to be simulated by the test and can be described by low cycle fatigue (LCF) and high cycle fatigue (HCF). The LCF loads consist of an axial shaft force and a shaft torque whereas the HCF loads are made up of a constant gyro bending moment and cyclic torque, the latter being superimposed to and varying the LCF torque.

For that purpose, the non-rotating LP shaft was fixed with the dummy fan disc end to a support plate, while at the other end the cyclic fatigue loads (axial tension, torsion, rotating bend) were introduced (Figure 2.10). The introduction of load occurs via a steel cylinder, clamped to the end of the LP turbine shaft. Axial tension and torsion are applied by hydraulic actuators, the rotating bend is introduced by two hydraulic torque motors arranged at an angle of 90 degrees relative to another.

The resulting axial and torsion strains, generated in the shaft, were measured by correspondingly applied linear strain gauges. The bending deformation was measured by two displacement transducers.

The test rig has been placed on IABGs modular test area (MTA), providing a rigid area for fixation and hydraulic supply stations for the actuators.

A total of 88.000 LCF cycles, each containing 134 HCF cycles were applied during the test.

Figure 2.10 MTA with the non-rotating LP shaft and hydraulic actuators

2.9 Rolls-Royce BR725 - Rear Mount Ring Static and Fatigue Tests

O. Tusch and G. Hilfer (IABG)

The titanium rear mount ring (RMR) of the Rolls-Royce BR725 engine is currently exposed to a series of static tests and fatigue testing at the IABG test laboratories in Ottobrunn, Germany.
The test specimen has already been tested statically to demonstrate the strength of the rear mount ring and to compare the experimental results with the FEM calculation.
In 2009, the fatigue test will be performed in order to fulfil the certification requirements of the rear mount ring.
The test specimen was integrated between two CFRP dummies. IABG was responsible for the design and production of these dummies which needed to have a stiffness equivalent to the adjacent a/c bypass duct structure and the a/c thrust reverse unit. The specimen is loaded by 16 hydraulic actuators, acting onto both the inner and outside of the rear mount ring structure and onto the dummies. The inner diameter of the test article and the number of actuators defined to apply the internally acting loads required high efficient usage of the available space.

The test specimen has been equipped with 63 strain gauge channels and 24 displacement transducers. Later this year the test specimen will be exposed to fatigue and damage tolerance testing.

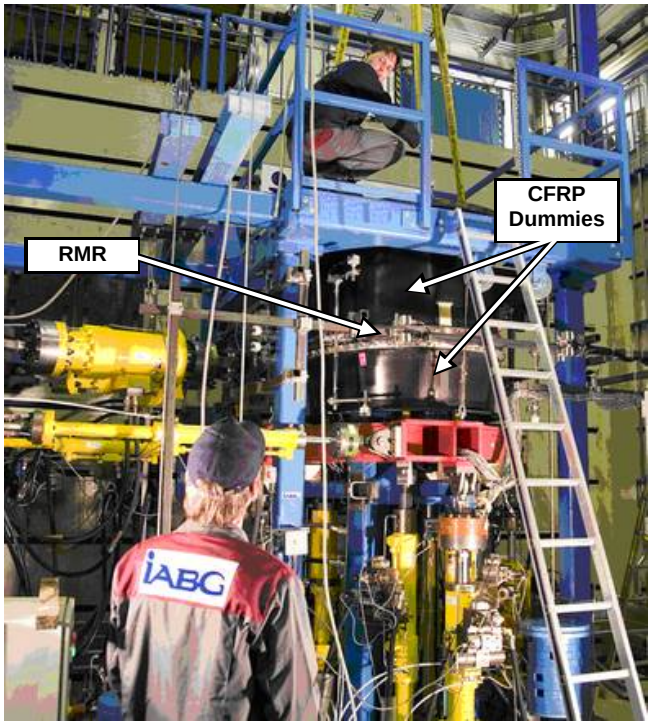

Figure 2.11 Test Set-up of the BR725 Rear Mount Ring test

2.10 Fatigue Test of the Tornado NLG Backup Structure

P. Böer and G. Hilfer (IABG)

In the years 1980 to 1998, a major airframe fatigue test (MAFT) of the structure of the Panavia 200 Tornado aircraft has been performed. After reaching of approximately 21.000 test hours the entire test was stopped and continued with component tests of particular parts of the MAFT specimen.
One of these tests is a fatigue test on the nose landing gear (NLG) backup structure.
The present qualification goal of the landing gear and its backup structure has been proven in the past by fatigue tests such as MAFT. The in-service usage in the air forces however has led to extended qualification requirements which should be obtained from a component test. The test should comprise additional “test full stop landings” and “test retraction and lowering cycles”.
The test was started in 2003 and was stopped in 2006 after several damages in the backup structure had been found. Since similar damages were found in in-service aircraft, a repair solution for the affected parts is currently being developed. After the introduction, the test will be continued to qualify this repair.
In the test, the NLG leg and the backup structure are loaded by seven hydraulic actuators. Five actuators are connected by a load introduction device at the wheels of the leg to simulate the landing loads. They are reacted by two actuators installed at the backup-structure before and after the NLG bay and by six struts of the restraint system of the MAFT. The original retraction jack has also been installed and is used to simulate the retraction and lowering loads. The set-up is shown in Figure 2.12.

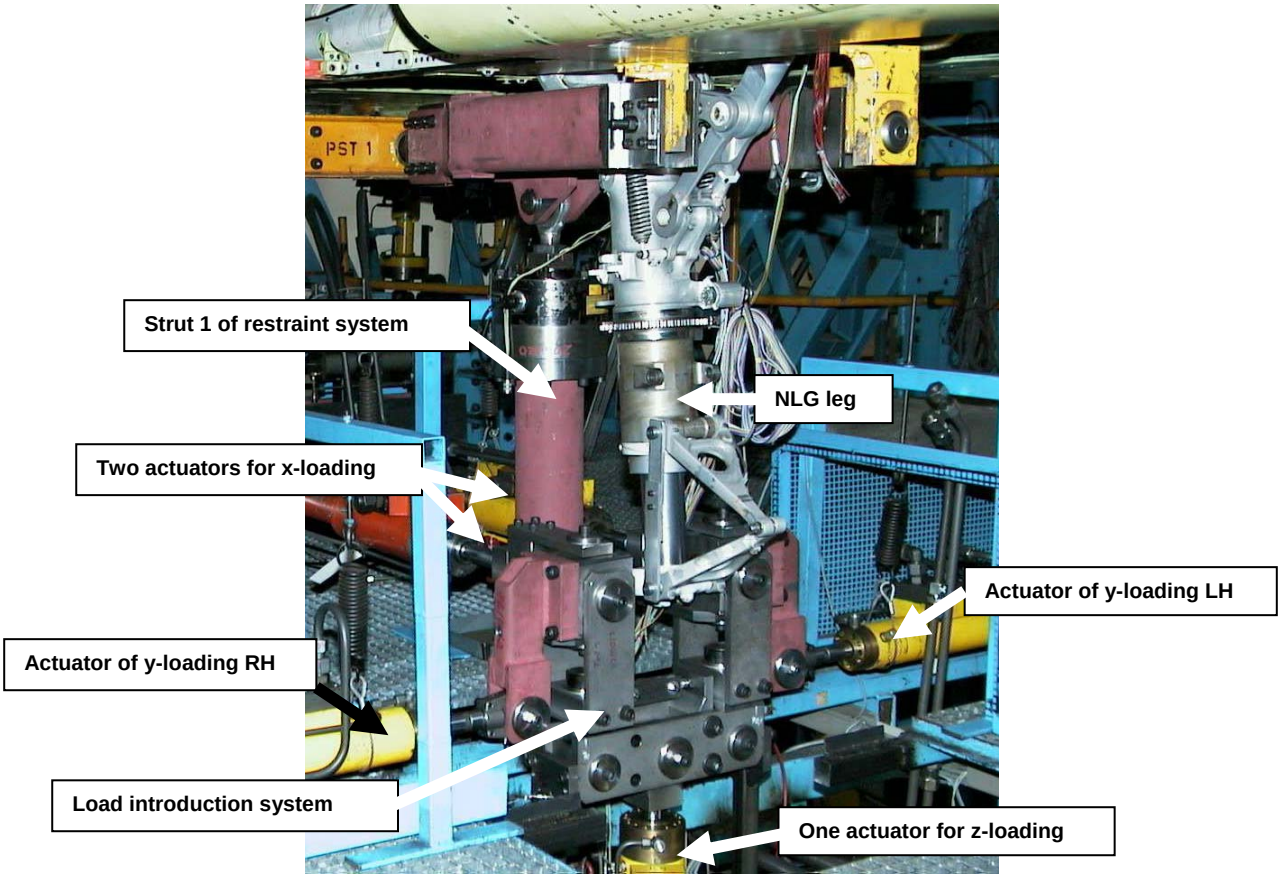

Figure 2.12 Set-up of Nose Landing Gear Test

The test programme of the fatigue loading is a randomized flight-by-flight programme consisting of different operational load cases combined to seven flights. In order to simulate the retraction and lowering loads into the backup structure correctly, the original NLG leg is frequently replaced by a steel dummy loaded with the retraction jack only.
Daily visual inspections and NDI at defined intervals were carried out to find damages in the structure. Additionally strain gauge measurements were performed during the test to examine the ageing behaviour of the structure.

3 Fatigue and Fracture of Fuselage Panels and Joints

3.1 Fatigue Crack Growth in FSW Joints Subjected to In-phase Biaxial Loads

F. Rubitschek (Uni-Paderborn), C. Sick (DLR), K.-H. Trautmann (DLR) and G. Biallas (HAW)

Both butt joints and stiffened panels with overlap-welded stringers were friction stir welded from AA 2024-T3. Fatigue cracks growing from saw-cuts oriented parallel to the joint line were inspected under in-plane biaxial load. To resemble the situation of pressurized fuselage structures, proportional loading without any phase shift, but with different biaxial load ratios λ was applied.

$$\lambda = \frac{load\ \ parallel\ to\ the\ crack\ \ plane}{load\ \ normal\ to\ the\ crack\ \ plane}$$

For example: cracks in the crown section of a pressurized fuselage experience a biaxial load ratio λ very close to 0.5 or 2, if they are oriented in axial or circumferential direction, respectively. The cruciform specimen used for the present study is shown in Figure 3.1.
Usually, a higher stress component parallel to the crack diminishes plastic zone size and crack opening displacement at maximum load [1]. For butt joints, however, increasing the biaxial load ratio from 0.5 to 1 only resulted in a small increase in fatigue life (Figure 3.2). Obviously, the positive effect of the higher biaxial load ratio was partly counterbalanced by the concurrent increase in maximum principal stress. Fatigue life of stringer specimens even decreased when increasing λ from 0.5 to 1 (Figure 3.2). Probably, the stringer has partially shielded the saw-cut from the life-increasing load component in crack growth direction. Comparing biaxial load ratios 1 and 2 revealed a pronounced increase in fatigue life for the higher λ (Figure 3.2). This was to be expected as the crack-driving load component perpendicular to the saw-cut was halved.
Using the definition of Cotterell and Rice [2], the initial direction of the small crack formed at the starter notch is an imperfection that will cause the crack path to permanently deviate from the straight starter when λ > 1, whereas it has only a local effect on the path when λ < 1. These features are consistent with the present experimental results in Figure 3.3, where fatigue crack initiation at the straight starter notch is shown for the two most opposite test conditions. For λ = 0.5, the crack in the stringer specimen turned back to straightness, whereas crack tips curved away from the starter and the long crack trajectory became S-shaped for λ = 2 (Figure 3.3). Further information on long crack paths can be found in [4].

Mixed mode I and II crack growth was reported to be prevalent when λ ≠ 1 and the crack simultaneously deviates from the direction of the starter notch [5]. In the present study, both conditions were fulfilled for the loading at λ = 2, and therefore, the approach of Leevers et al. [3] that is also valid for mixed mode crack growth was applied to calculate stress intensity factors. For 20 MPa√m < ΔK < 60 MPa√m, corresponding da/dn-ΔK curves were situated in a common scatter band (Figure 3.4). In spite of the totally different fatigue life and crack path (*cf.* Figure 3.2 and Figure 3.3), this also applied to the butt joint specimen loaded at λ = 2.

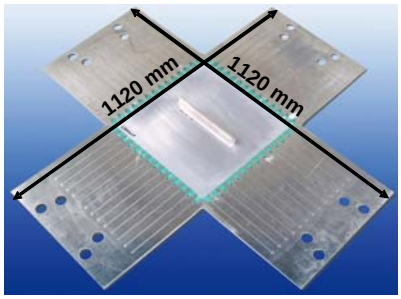

Figure 3.1 Cruciform specimen

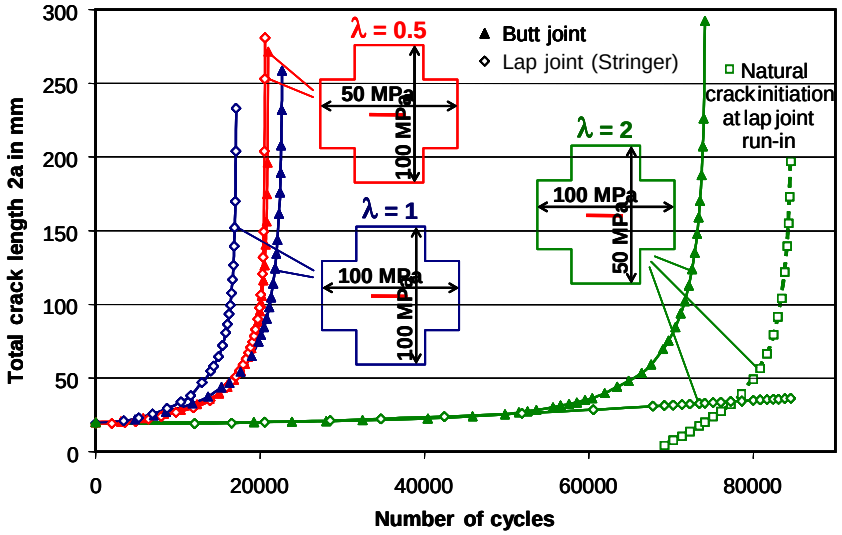

Figure 3.2 Crack growth for butt joint and stringer specimens loaded biaxially as indicated (starter notch parallel to the weld seam)

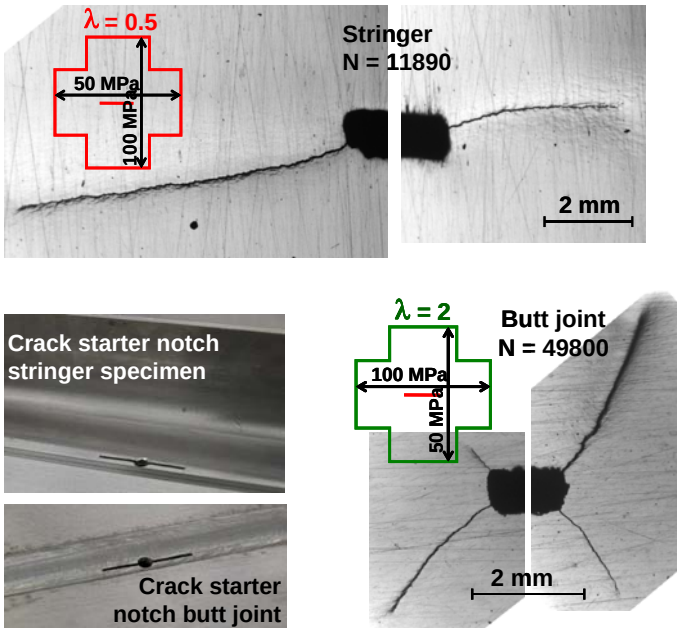

Figure 3.3 Crack starter and crack initiation at the starter notch as observed on specimen back side for loading conditions as indicated

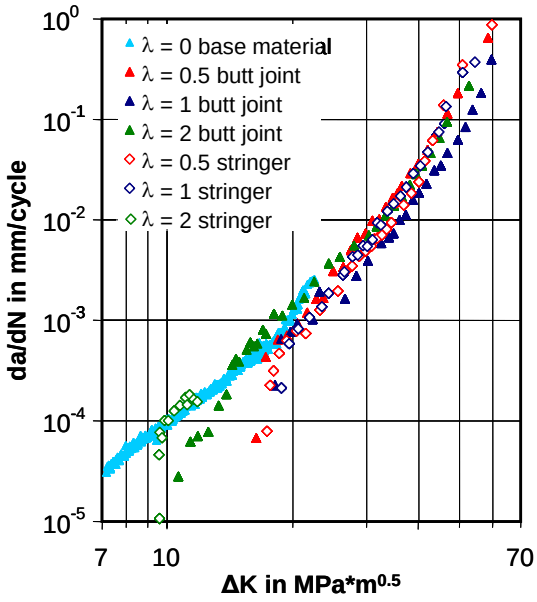

Figure 3.4 da/dn-ΔK curves calculated according to Leevers et al. [3], reference data from uniaxially loaded base material

References

[1] N. J. I. Adams (1973) *Engng Fract. Mech.* 5, 983.
[2] B. Cotterell, J. R. Rice (1980) *Int. J. Fract.* 16, 155.
[3] P. S. Leevers, J. C. Radon, L. E. Culver (1976) *J. Mech. Phys. Sol.* 24, 381.
[4] F. Rubitschek, C. Sick, K.-H. Trautmann, G. Biallas (2008) in *Aluminium Alloys – Their Physical and Mechanical Properties* (Eds.: J. Hirsch, B. Skrotzki, G. Gottstein), Wiley-VCH, Vol. 2, 1570.
[5] E. W. Smith, K. J. Pascoe (1983) *Fat. Engng Mater. Struct.* 6, 201.

3.2 Improvement of Damage Tolerance of Laser Beam Welded Aluminum Panels via Crenellations

M.-V. Uz (GKSS), M. Koçak (GKSS), F. Lemaitre (ALCAN CRV), J.-C. Ehrström (ALCAN CRV), S. Kempa (ALCAN T&M) and F. Bron (ALCAN CRV)

In order to improve the fatigue life, systematic thickness variations (crenellations) were introduced onto the skins of laser beam welded stiffened panels. The weight of the crenellated panels was exactly equal to the reference panels for comparison. For a skin crack, the new design resulted in constitution of a fully modified stress intensity factor (SIF) profile such that SIF takes substantially lower values at certain locations and substantially higher values at some other locations compared to the reference geometry (Figure 3.5).

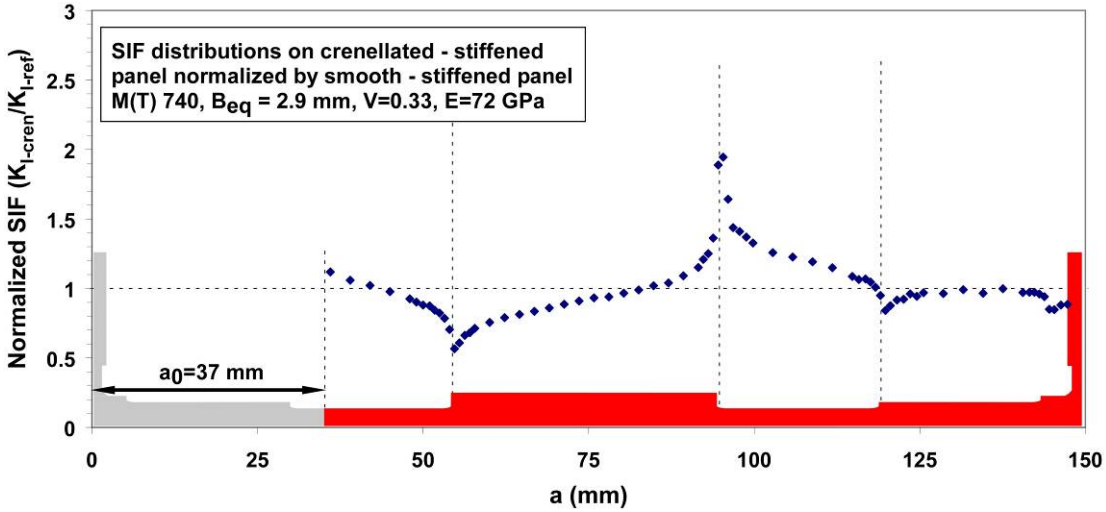

Figure 3.5 Mode I stress intensity factor (K_I) profile for a centre crack on a 740 mm wide aluminium panel with five laser beam welded stringers. Values were normalized with the values for a smooth reference panel of equal outer dimensions and weight

These sharp SIF fluctuations on crenellated panels leaded to the formation of an “overload like” state even under constant amplitude loading conditions [1]. For example, wherever there is a negative slope on SIF profile, the fatigue crack growth rate sharply dropped due to the larger plastic zones formerly created. Experiments showed that, the fatigue crack growth life improvement due to crenellations is up to 65% under constant amplitude loading and even up to 150% under spectrum (modified Mini-TWIST) loading conditions (Figure 3.6).

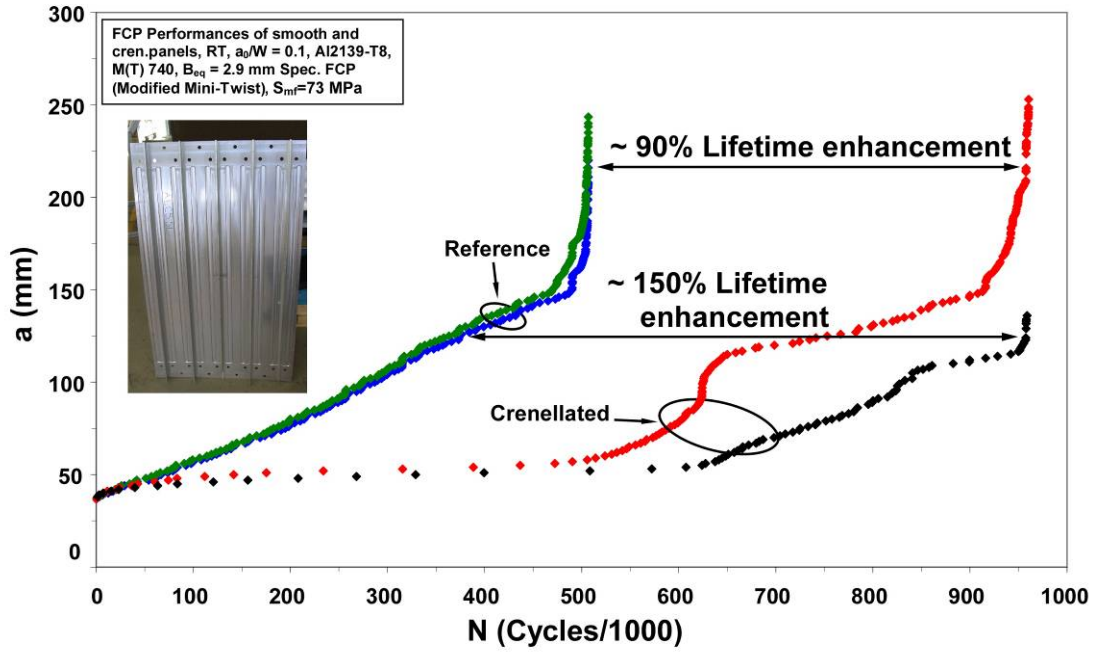

Figure 3.6 Crack length vs. number of fatigue cycles diagram for reference and crenellated panels tested under modified mini-TWIST spectrum showing the substantial fatigue life improvement due to crenellations

References

[1] M.-V. Uz, M. Koçak, F. Lemaitre, J.-C. Ehrström, S. Kempa, F. Bron, “Improvement of damage tolerance of laser beam welded stiffened panels for airframes via local engineering” International Journal of Fatigue 31 (2009), 916-926

3.3 Experimental Investigation on Bonded Structures for increased Damage Tolerant Aircraft Structures

I. Meneghin (Uni-Bologna), P. Vermeer (EADS-IW) and M. Pacchione (Airbus)

Adhesive bonding provides solutions to realize cost effective and low weight aircraft fuselage structures in particular where the damage tolerance (DT) is the design criteria. Bonded structures that combine metal laminates (MLs) and eventually selective reinforcements can guarantee slow crack propagation, crack arrest and large damage capability.

MLs are produced by adhesive bonding of a number of thin sheets to obtain the required thickness; the laminate may incorporate bonded local reinforcements. Selective reinforcements expand the local reinforcement’s concept using fatigue insensitive materials to further improve the crack growth and residual strength performances.

To optimise the design exploiting the benefit of bonded structures incorporating selective reinforcement requires reliable analysis tools. The effects of bonded doublers / selective reinforcements is very difficult to be predicted numerically or analytically due to the complexity of the underlying mechanisms and failures modes acting: debonding at the interface between the doubler and the skin around the crack tip, load redistribution between damaged part and intact

reinforcements, fatigue damage of the metallic reinforcement eventually causing its premature failure, crack bridging of long crack in case of fatigue insensitive doublers. In addition, secondary effects like tensile residual stresses from the bonding process and secondary bending due to the eccentric doublers increase the complexity of the phenomena.
Reliable predictions of crack growth can only be based on sound empirical and phenomenological consideration strictly related to the specific structural concept. With the purpose of investigating solutions applicable to pressurized fuselages large flat stiffened panels that combine MLs and selective reinforcements have been tested in frame of the EU Project (6th Framework Programme, No. 502846) DIALFAST - Development of Innovative and Advanced Laminates for Future Aircraft STructures.
The large test campaign (for a total of 35 stiffened panels) has quantitatively investigated the role of:

- different metallic skin concepts (monolithic vs. MLs)
- aluminium, titanium, glass-fibre reinforcements
- stringers material and cross sections
- geometry and location of doublers / selective reinforcements.

The performances of the different structural concepts are compared in terms of fatigue crack propagation over broken stringer and residual strength (2 bays crack).

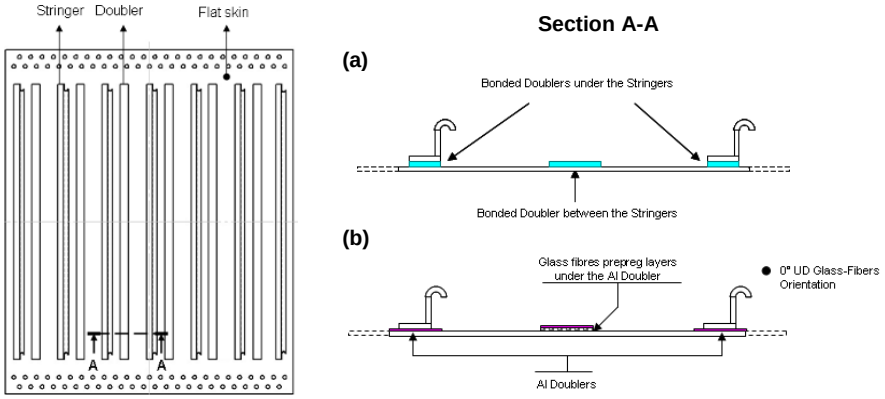

Figure 3.7 Test coupon: "seven stringers" panel with (a) doublers bonded between and below the stringers, with (b) additional glass fibre reinforcement

Bonded doublers and selective reinforcements confirmed to be outstanding tools to improve the DT properties of structural elements with a minor weight increase.

- The effectiveness of the metallic doublers is dominated by its fatigue crack nucleation period
- Aluminium doubler geometry/weight can be optimised to retard crack nucleation (thick and narrow instead of thin and wide)
- Bonding aluminium doublers with glass fibre reinforcements prevent fatigue nucleation creating a fatigue insensitive reinforcements
- Titanium doublers provide the advantage of high stiffness and long fatigue nucleation period. These advantages are to a certain extent reduced by the internal stresses created during hot bonding process
- Selective reinforcements (titanium or glass-fibre) may significantly increase residual strength

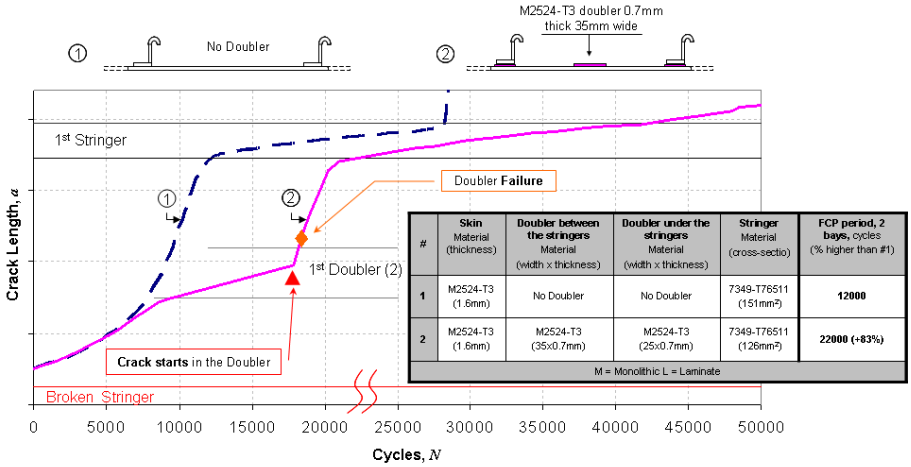

#	Skin Material (thickness)	Doubler between the stringers Material (width x thickness)	Doubler under the stringers Material (width x thickness)	Stringer Material (cross-sectio)	FCP period, 2 bays, cycles (% higher than #1)
1	M2524-T3 (1.6mm)	No Doubler	No Doubler	7349-T76511 (151mm²)	12000
2	M2524-T3 (1.6mm)	M2524-T3 (35x0.7mm)	M2524-T3 (25x0.7mm)	7349-T76511 (126mm²)	22000 (+83%)

Figure 3.8 Effect of aluminum bonded doubler in the middle of the stringer bay

The tests confirmed the considerable role of the skin/stringer material; however ML skin provides negligible advantages in terms of through crack propagation. The role of stiffener section as determined by tests is in good agreement with prediction based on displacement compatibility analysis. The crack retardation mechanisms, based on local stiffening and crack-bridging effects will be discussed for the different reinforcement concepts.

3.4 The Effect of Bonded Doublers on Fatigue Crack Initiation/Propagation in Longitudinal FSW Joints in Fuselage Panels

P. Vermeer, E. Hombergsmeier and V. Holzinger (EADS-IW)

Within the 6th European framework programme project “DIALFAST” (acronym for “development of innovative and advanced laminates for future aircraft structures”), the overall objective was to develop new and improved metal laminate (ML) concepts for aircraft fuselage structures.
One of the work packages was dedicated to the investigation of suitable joining methods for metal laminates, contributing to the improvement of mechanical performance with a simultaneous reduction of manufacturing costs of ML structures in comparison to the conventional monolithic metallic design.

Friction stir welding (FSW), e.g. in order to replace splicing in ML, has been selected as an innovative concept for a longitudinal joint in the fuselage skin. Normally, for ordinary butt welds in primary structures, tapered gusset plates ensure a gradual change and a reduction of the stress intensity in the welded members, lessening the danger of (fatigue) failure. In thin sheet MLs however, tapered panels are unfavourable and an adhesively bonded doubler will be used instead. The doubler’s function is to pick-up and bypass load, relieving this to the other member lowering the stress intensity in the weld.

The aluminium panels have been welded, the surfaces pretreated and doublers autoclave bonded with an epoxy-based structural film adhesive. The schematic representation of the lay-up (Figure 3.9) shows the variation in doubler sizing for monolithic welded panels and ML spliced skin.
Both fatigue crack initiation (FCI) samples and M(T) specimens for fatigue crack propagation (FCP) have been machined and tested.

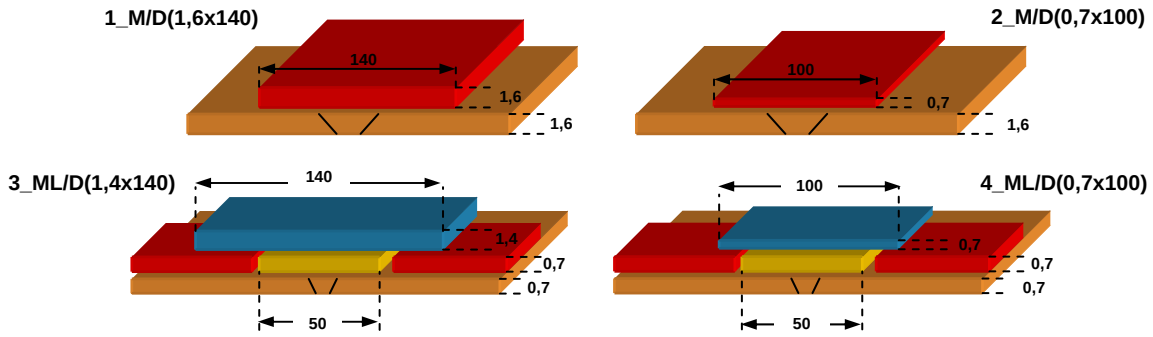

Figure 3.9 Schematic representation of the FSW panels

The Wöhler curves of the monolithic specimens in Figure 3.10 show a clear positive influence of the thin doublers, although initiation did generally occur in the base panel at the doubler edge far away from the weld, where the stress intensity is highest. The ML samples showed early FCI in the metal layer closest to the doubler and after a certain propagation time retarded crack initiation in the second layer. This crack will be able to propagate without retardation through-thickness in case of a monolithic skin. Therefore, generally the FCI behaviour of the ML samples is significantly better than that of the monolithic ones.

Considering FCP in ML panels, it was quite challenging to initiate a single fatigue crack in the welded area, but finally the M(T) specimens failed starting from the pre-cracked area along the line of welding, also cracking the bonded doubler. No large delamination was observed. The ΔK–*da*/*d*N curve plotted in Figure 3.11 shows the doubler effect on FCP in ML panels 3 and 4. ΔK has been calculated according to ASTM–E647 even if the requirement of a homogeneous specimen is not met:

$$\Delta K = \frac{\Delta P}{B}\sqrt{\frac{\pi a}{2W}\sec\frac{\pi a}{2}}\text{, where } \alpha = 2a/W$$

The doubler effect in FCP is observed being the reverse of the FCI tests; regarding the ΔK related to the base skin-thickness only, a thick doubler is beneficial for crack propagation due to the reduced stress intensity. However even the lay-up with the thin doubler could meet the requirement, demanding equal FCP in comparison to a monolithic non-welded skin.

If the entire ensemble, i.e. skin *and* doubler is taken into account (represented by *open* markers in Figure 3.11), the crack tip is considered to be in a different stress state and crack bridging effects give a marginal advantage to the thin doubler. The 2a-N plot (Figure 3.11) shows a +90% increase in lifecycles when applying a thick doubler.

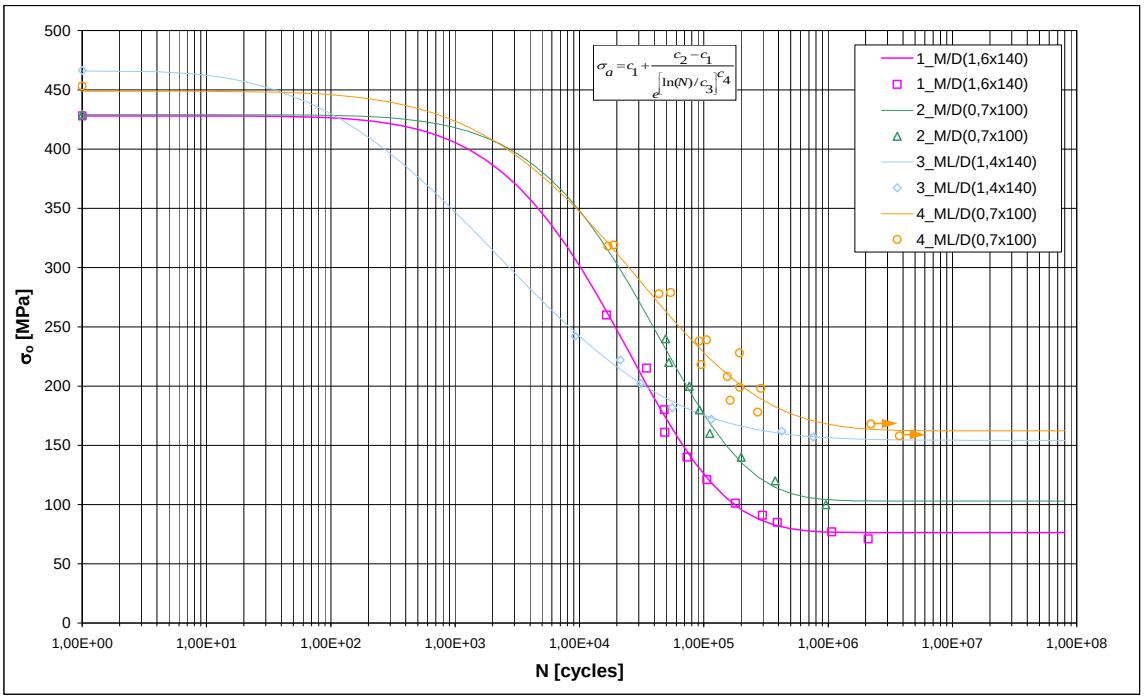

Figure 3.10 S-N curve for FSW panels comparing bonded doubler geometry

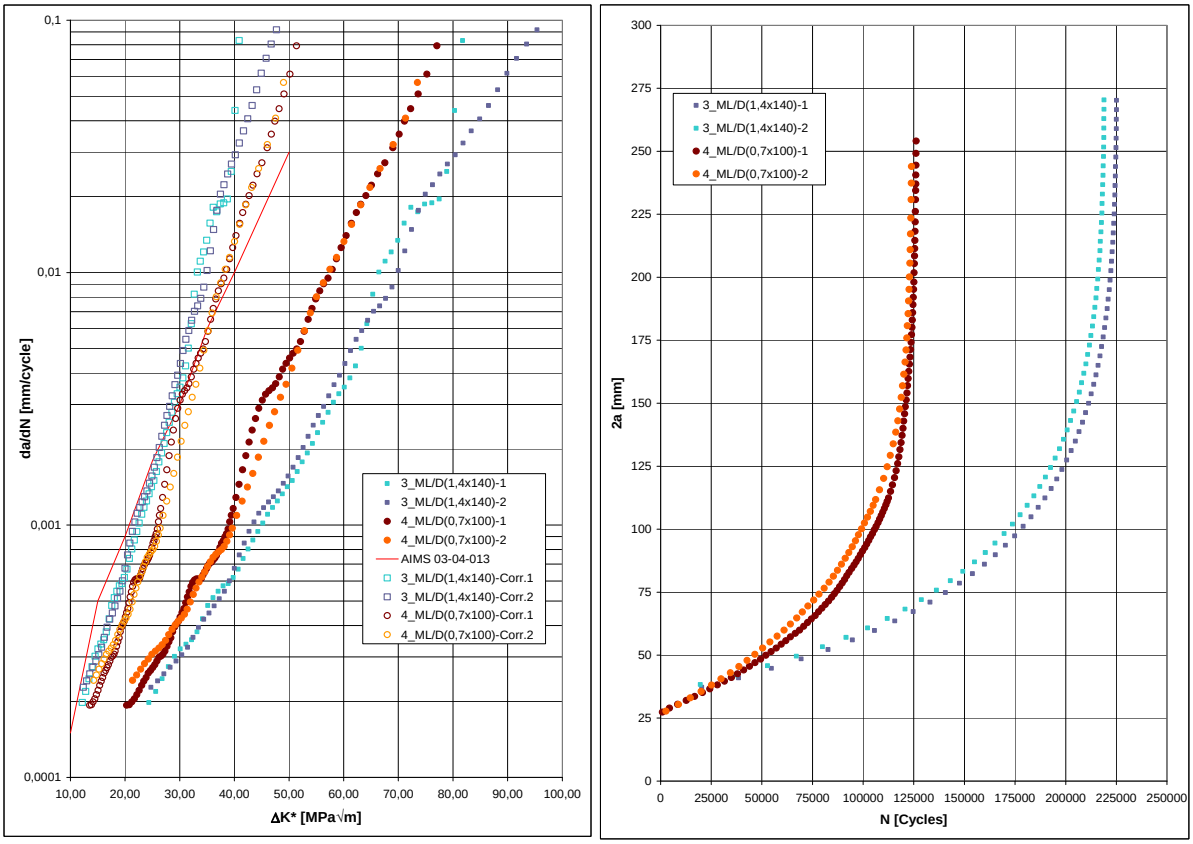

Figure 3.11 Left: ΔK*–da/dN curve for FSW panels and Airbus reference (AIMS). ΔK* with doubler correction (open markers). Right: 2a-N curve for FSW panels until failure, calculated stress correction for panel 3.

3.5 Bonded Repair for Fuselage Damage: an Overall Benefit to Commercial Aviation

D. Furfari (Airbus), H.J.M. Woerden (Shell), R. Benedictus (TU Delft) and A. Kwakernaak (TUD-AI)

Adhesively bonded repair of aircraft structures is frequently used in military applications, especially with the Australian and United States Air Forces. Although bonded repairs have the capacity to provide a maintenance-free repair solution to a variety of structural damages when compared to conventional mechanically fastened repairs, commercial operators still only use them on a very limited scale.
In this paper the fatigue behaviour of bonded repairs to aluminium fuselage skins structures are discussed. A fatigue test campaign with increasing complexity of the test specimen ("pyramidal approach") was carried out. Fatigue test results of cold and hot bonded repairs were compared to those of conventional riveted repairs. Two types of environmental conditions during application of bonded repairs have been considered: the "production" environment meaning a bonded doubler with surface pre-treatments and bond line curing conditions as will be used in production environment (Grit-blast Silane, autoclave); and the "repair" environment as the one typical when a repair is applied to an aircraft in-field (SolGel® surface pre-treatment, vacuum bag and heat blanket).
Tests ranged from simple coupon specimens (butt-joints) to aircraft structural components (curved stiffened fuselage panels), in which both a conventional riveted repair and the hot bonded repair were embodied. Flat unstiffened panels with increasing cutout (i.e. damage) size were also tested using the different bonded repair solutions. All specimens were subjected to constant amplitude fatigue loading at stress ratio R=0.1. The applied loading conditions of the curved stiffened panels were internal pressure and longitudinal load at R=0.1, simulating in-service loading conditions of an aircraft fuselage. The fatigue life of the conventional riveted repair was used as reference to estimate the fatigue life enhancement for the bonded repairs.

The influence on fatigue life of surface pre-treatment, environment ("production" or "repair") as well as adhesive type (cold or hot bonding) was studied. The results of the coupon specimens were used as input for design of the next specimen type in the "pyramidal approach" by selecting the combination of the parameters showing the most promising and most interesting results. The bonded repairs on the curved stiffened fuselage panels were applied using SolGel® as surface pre-treatment, and a vacuum bag and heat blanket cure setup to simulate in-field repair conditions as will most usually be met with for a real aircraft.
It was found that the amount of cycles to initiate a fatigue crack in bonded repair solutions on the coupon specimens strongly depends on the adhesive type used. The fatigue lives of cold bonded coupon specimens were not longer than that of the reference riveted repair. The hot bonded coupon specimens showed a significant enhancement in fatigue performance with fatigue lives up to 6 times longer than the conventional riveted repair. In general the hot bonded repair solution, regardless of the surface pre-treatment or the application environment showed a fatigue life at least 2 times longer than the reference riveted repair solution. These results were confirmed for hot bonded repairs applied to the most realistic (top of the "pyramid") curved stiffened fuselage panel specimens.

3.6 Hybrid Structure Solution for the A400m Wing Attachment Frames

M. Plokker, D. Daverschot and T. Beumler (Airbus)

The mainframes in the centre fuselage of A400M have the vital function of introducing the wing loads into the fuselage. The lift distribution among the wing causing a torque and the frame curvature causing a bending moment, result in high running stress and limit loads in the frames below the rear wing attachment. These frames are made of 7000 aluminium alloy and are therefore primarily dimensioned by fatigue reasons, especially crack growth.
Consequently, three different options for the A400M mainframes have been investigated to fulfil the fatigue, maintenance, and weight targets. The investigation was focused to reinforce the inner flanges of the frames. The inner flange is the highest loaded and critical part of the frame.

Three reinforcement options were investigated:

1. Thickening of the aluminium inner flange to reach an acceptable stress level
2. Application of riveted Titanium strap attached to inner flange
3. Application of bonded Glare® strap attached to inner flange

In the option 2 and 3, the strap acts as damage containment feature that redistribute the load in case of a damaged frame. The first part of the investigation was the comparison of the three designs on weight, fatigue behaviour, and cost. A coupon test program was performed to investigate the behaviour of aluminium reinforced with bonded Glare® strap. This shows a constant crack growth rate for long ranges of crack lengths (in contrary to aluminium or titanium reinforced inner flange). The inspection and cost requirements of the bonded Glare® strap reinforcement are well within the programme boundaries. Additionally, the Glare® reinforced aluminium inner flange offers a weight opportunity of almost 20 kg's.

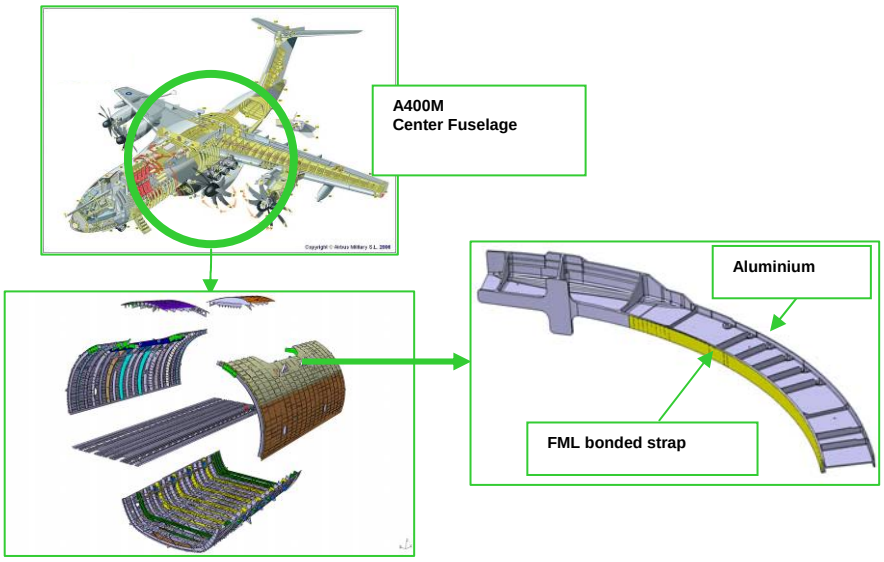

Figure 3.12 The A400M fuselage with the centre section and the division of the centre section

The certification of this application on A400M will be achieved by a series of coupon, component and the full-scale fatigue test. The local metal bonding process on a large part with complex contour is considered as challenging. Therefore a series of experiments is carried out to investigate the effect of artificial delamination and defects below the detection size in the

frame/strap bondline. A detailed finite element investigation is being done to determine the maximum size of delamination that sustains limit load condition. This analysis is validated by panel component testing. Completing the design philosophy, manufacturing process and certification of this particular application, anti peeling fastener will be installed locally, i.e. in rivet pitches that equal the determined maximum artificial delamination length.

3.7 Dialfast - Curved Fuselage Panel Fatigue and Damage Tolerance Test

H. Bause (IMA)

In frame of the EU project DIALFAST, a curved panel has been tested. The specimen was a curved fuselage panel composed of a metal laminate skin with a longitudinal friction stir weld, seven riveted frames and 10 bonded stringers. The metal laminate skin featured a waffle plate and consisted of three aluminium layers alternated with adhesive film. The skin was reinforced in circumferential direction and below the frames by fibre prepreg with different thickness. The panel included two unconventional longitudinal joints; one FSW splice and one metal bonded splice. It was one-dimensionally curved with a radius of 2820 mm corresponding to the radius of an A340 type a/c, despite the fact that the panel design was representing a Single Aisle fuselage with a minimum skin thickness of 0.8mm.
The objective of the test was to obtain relevant fatigue and damage tolerance data and it has been realized on the IMA test rig “V0” (Figure 3.13), which is assembled modularly and consists of a pressure box and rig. The pressure box allows the application of the aircrafts internal pressure to the panel, creating a biaxial stress condition in collaboration with a longitudinal force. In order to prevent the frames from bending, a force is applied to the edges representing a linear function of the internal pressure.
The specimen has been equipped with strain gauges and fibre Bragg gratings. Prior to the fatigue tests, a static test has been performed to serve the definition of loads. The fatigue test consisted of both sine cycling and flight spectrum; the first 60.000 cycles were sinusoidal loading only, subsequently, four artificial damages have been introduced and their crack propagation behaviour monitored. Again, the loads had been applied as flight spectrum or sinusoidal.
The artificial damages were saw cuts both hoop and lengthwise, with and without damaging close-by stiffening elements such as stringers and frames. Of special interest was the influence of integrated fibres on the crack growth direction and rate. As expected, the cracks grew mainly along the fibres orientation, clearly visible from the observation of one crack cutting through a frame. This specific crack expanded after introduction, following the stringer orientation, corresponding to cracks in longitudinal direction in order to traverse the area between 2 frames. By reaching the vicinity of the next frame, the crack was deflected by the underlying fibres moving the crack continue to grow along the frames. This crack growth behaviour was intended to improve the damage tolerance behaviour. By deflecting the crack between 2 frames, a “flap” is created which will lower the crack driving load component when opening as a result of internal pressure by blowing off the remaining internal pressure. As could be shown in a residual strength test, the crack formed exactly that flap which led the internal pressure to drop, Figure 3.14.

Figure 3.13 IMA Test-rig V0

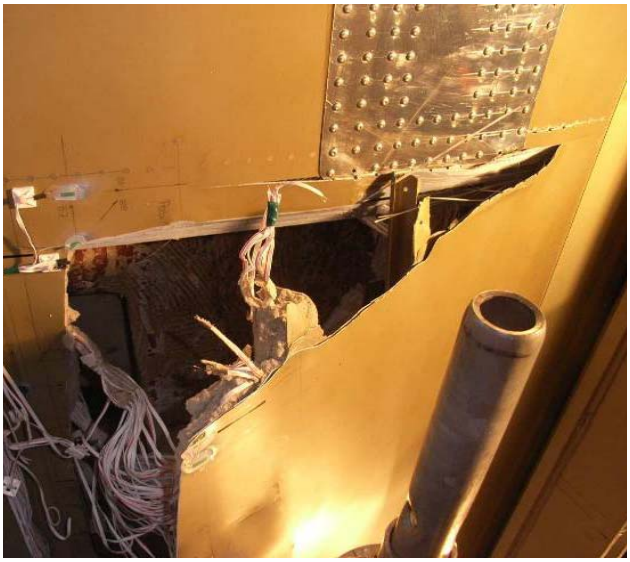

Figure 3.14 Flap after residual strength testing

3.8 Performance of Fatigue Crack Initiation and Propagation Tests for Supporting Assessment of Repair Solutions in Riveted Glare Joints

J. Bolten and G. Hilfer (IABG)

The aim of these tests was to provide an experimental background for the assessment of repair solutions for scratches deeper than one aluminium layer in riveted GLARE longitudinal joints.
The test program made use of two different kinds of materials (Standard GLARE and HSS GLARE) and two different kinds of repairs (dimple and protective sheet). The specimens consisted of riveted lap joints with three rivet rows of five rivets each. Several batches were exposed to static and fatigue testing.
One specimen of each batch was statically tested in maiden condition. The specimens were instrumented with an extensometer in order to produce a load verses displacement curve.

The fatigue tests were divided in three test phases – crack initiation tests, crack propagation tests and residual strength tests.
To create a Wöhler curve the specimens were exposed to fatigue loading at different load levels. The point of crack initiation was defined as an average crack length of approx. 1mm whereas the 10 fatigue sensitive locations in the highest loaded rivet row of one sheet were considered.

In order to define crack initiation accurately and efficiently, several specimens of each batch were equipped with special vacuum foil sensors. The sensors were applied inside the lap joint area around the bore hole of the first and third rivet row and connected to a comparative vacuum monitoring system (CVM). The servo-hydraulic testing machine (Schenk 160kN) was

automatically stopped once a crack was detected by the CVM sensor. The specimens were carefully disassembled and a non-destructive inspection was executed using the high frequency eddy current testing (HFET). All crack lengths were determined and crack locations and crack lengths were recorded. Based on these results a preliminary Wöhler curve was established which allowed a directed test continuation of the remaining specimens without any further application of CVM sensors.

After crack initiation tests the specimens were reassembled and two crack propagation tests per specimen followed. Aim of the crack propagation test phase was to create an average total crack length of approx. 5-7mm. The specimens were disassembled after each crack propagation test. The inspection and measurement of the cracks was carried out similarly to the crack initiation phase.

Following the crack propagation tests all specimens were pulled to failure to determine the residual strength. The specimens were instrumented with an extensometer in order to produce a load versus displacement curve.

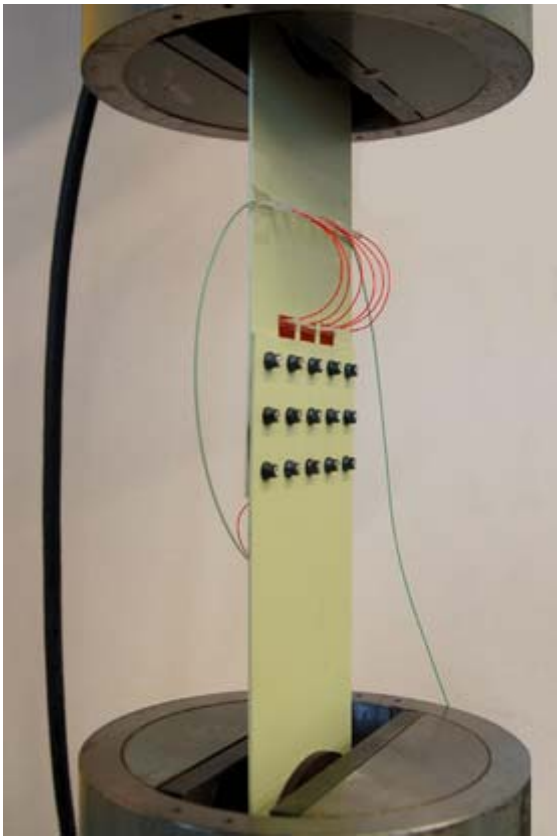

Figure 3.15 Riveted GLARE longitudinal joint specimen with integrated vacuum foil sensors

4 Fatigue Life Assessment and Prediction

4.1 General Reliability Theory in Elastic Mathematics

L.G. Gelimson (IFST)

Traditional mathematics [1] brings key concepts that are very often insufficient, have evident lacks, and are not suitable for solving many typical problems. For example, to estimating reliability, a stochastic approach [1] often applies. Also in deterministic problems, their parameters are often artificially randomized. The corresponding distributions are considered known (even if they are really unknown) and most suitable for calculation. But even such a simplification brings complicated formulae and difficulties by analysis.
Elastic mathematics [2] based on the principles of natural thinking brings many new general theories suitable for science, engineering, and life. Among them is general reliability theory.
The ***reliability*** of an object (e.g., element, structure, etc.) can be naturally defined as the probability that the object *holds* in some reasonable sense (e.g., exists and successfully functions during a given time interval under certain conditions such as loading, temperature, etc.). The above object can take so called ***values*** as its particular states, realizations, etc. which are any objects, too. A value is called ***admissible*** if the object taking this value holds. A value is called ***inadmissible*** if the object taking this value does not hold. A value is called ***limiting*** if it belongs to the common boundary of the admissible values and inadmissible ones. In other words, in each, arbitrarily small, neighbourhood (in a certain reasonable sense) of such a value, there are both admissible and inadmissible values. A limiting value is either admissible or inadmissible.
The actual value of the object can deviate from its nominal value corresponding to available information always incomplete, usually inexact, and sometimes partially unreliable. This can be not only quantitatively, but also qualitatively significant. The last can especially hold for the limiting values and values near to those in some reasonable sense. For example, by such an admissible, limiting, or inadmissible nominal value, the actual one can be admissible, limiting, or inadmissible in any combination of these properties.
The introduced reserve [2, 3] makes it possible for the first time, to also deterministically estimate reliability in many types of problems and to provide relatively simple formulae very suitable for analysis. Let us determine reliability S via reserve R (whose values belong to the closed interval [-1; 1]) as $S = (1 + R)/2$. Then the range of S is the closed interval [0; 1] like that of probability, which is natural. For admissible values (states etc.) of the object that are infinitely far from their boundary (its limiting values) in certain reasonable sense, $S = 1$. For the limiting values themselves, $S = 1/2$. For inadmissible values infinitely far from their boundary (its limiting values) in certain reasonable sense, $S = 0$. All these values of reliability are natural and correspond to intuition. For a limiting value, due to possible deviations from it in the reality, the value of a parameter with risk can also be either admissible or inadmissible. It is reasonable to consider equal the measures, probabilities, and some similar estimates (e.g., multi-quantities [2]) of the both kinds of the deviations. The same estimates of the limiting values only can be regarded as infinitely small in comparison with the previous both because the dimension of the above boundary (the set of the limiting values) is usually less than the dimension of the set of the admissible values and that of the inadmissible ones. In the one-dimensional case, e.g., for a unique real parameter, the boundary typically consists of some discrete values and is zero-dimensional whereas both the set of the admissible values and the set of the inadmissible values are one-dimensional.
Example. Both $x_1 = 1 + 10^{-10}$ and $x_2 = 1 + 10^{10}$ are exact solutions to the inequation $x > 1$, x_1 practically unreliable and x_2 guaranteed. Their discrimination is especially important by any inexact data. Traditional mathematics [1] cannot provide this at all. In elastic mathematics [2, 3], the reserve of any pseudosolution x to the combined inequations

$$[_{\alpha\in A}\, a_\alpha \Leftarrow x \Leftarrow b_{\beta\ \beta\in B}]$$

where a, b, x are real numbers, $\Leftarrow$ is one of the two inequality signs $<$, $\leq$, can be defined as [2]

$$R(x, [_{\alpha\in A}\, a_\alpha \Leftarrow x \Leftarrow b_{\beta\ \beta\in B}]) = \inf_{\alpha\in A,\ \beta\in B} ((x - a_\alpha)/(|x|+2|a_\alpha|+1), (b_\beta - x)/(|x|+2|b_\beta|+1)).$$

Then

$$S_{x>1}(x_1) = S_{x>1}(1 + 10^{-10}) = (1 + R_{x>1}(1 + 10^{-10}))/2 =$$
$$(1 + 10^{-10}/(2 + 10^{-10}))/2 = (1 + 10^{-10})/(2 + 10^{-10})$$

a little greater than 1/2 and

$$S_{x>1}(x_2) = S_{x>1}(1 + 10^{10}) = (1 + R_{x>1}(1 + 10^{10}))/2 =$$
$$(1 + 10^{10}/(2 + 10^{10}))/2 = (1 + 10^{10})/(2 + 10^{10})$$

a little smaller than 1, both in accordance with intuition.
Introduced reliability brings (also by distributions) adequate estimations of approximation quality, exactness confidence, and risk. The proposed general reliability theory is very effective by setting, reasonably simulating, and solving many types of problems in science and engineering including aeronautical fatigue.

References

[1] Encyclopaedia of Mathematics. Ed. M. Hazewinkel. Volumes 1 to 10. Kluwer Academic Publishers, Dordrecht, 1988-1994
[2] Gelimson, L. G.: Elastic Mathematics. General Strength Theory. The “Collegium” All World Academy of Sciences Publishers, Munich, 2004
[3] Gelimson, L. G.: General Reserve Theory. In: Review of Aeronautical Fatigue Investigations in Germany During the Period March 2003 to May 2005, (Ed.) Dalle Donne, C., SC/IRT/LG-MT-2005-039 Technical Report, Aeronautical fatigue, ICAF2007, EADS Corporate Research Centre Germany, 2005, 55-56

4.2 General Risk Theory in Elastic Mathematics

L.G. Gelimson (IFST)

For many typical problems in science and engineering including aeronautical fatigue, there are no concepts and methods adequate and general enough. Even artificially simplifying by randomizing parameters in deterministic problems to apply stochastic approaches in traditional mathematics [1] to estimating risk brings complicated formulae and analysis difficulties. Elastic mathematics [2] is very suitable for solving such problems and includes many general theories and methods. Among its new concepts are the autoerrors and reserves estimating and measuring also exactness, contradictoriness, and distributions. The autoerrors [2, 3] correct and generalize the relative error. The reserves [2] new in principle estimate exactness reliability. They both form a basis for general risk theory.
The ***risk*** of an object (e.g., element, structure, etc.) can be naturally defined as the probability of the event that the object *does not hold* in some reasonable sense (e.g., cannot exist and/or successfully function during a given time interval under certain conditions such as loading, temperature, etc.). The above object can take so called ***values*** as its particular states, realizations, etc. which are any objects, too. A value is called ***admissible*** if the object taking this value holds. A value is called ***inadmissible*** if the object taking this value does not hold. A value is called ***limiting*** if it belongs to the common boundary of the admissible values and inadmissible ones. In other words, in each, arbitrarily small, neighbourhood (in a certain reasonable sense) of such a value, there are both admissible and inadmissible values. A limiting value is either admissible or inadmissible.

The reserve [2] makes it possible for the first time, to also deterministically estimate risk in many types of problems in science, engineering, etc. and to provide relatively simple formulae very suitable for analysis.
Let us determine risk r via reserve R (whose values belong to the closed interval [-1; 1]) [2] as

$$r = (1 - R)/2.$$

Then the range of r is the closed interval [0; 1] like that of the autoerror (with certain sense similarity). By no risk we have r = 0. For a limiting value, r = 1/2. For inadmissible values infinitely far from a limiting value, r = 1. All these values of risk are natural and correspond to intuition. For a limiting value, due to possible deviations from it in the reality, the value of a parameter with risk can be either greater or less than the limiting value. It is reasonable to consider equal the probabilities, measures, and some similar estimates (e.g, multiquantities [2]) of the both kinds of the deviations whereas the same estimates of the only limiting value can be regarded as infinitely small in comparison with the previous both. The remaining cases r = 0 and r = 1 are trivial.
Example. Both

$$x_1 = 1 + 10^{-10}$$

and

$$x_2 = 1 + 10^{10}$$

are exact solutions to the inequation

$$x > 1,$$

x_1 practically unreliable and x_2 guaranteed. Their discrimination is especially important by any inexact data. Traditional mathematics [1] cannot provide this at all. In elastic mathematics [2, 3], the reserve of any pseudosolution x to the combined inequations

$$[_{\alpha\in A}\, a_\alpha \Leftarrow x \Leftarrow b_{\beta\, \beta\in B}]$$

where a, b, x are real numbers, $\Leftarrow$ is one of the two inequality signs $<$, $\leq$, can be defined as [2]

$$R(x, [_{\alpha\in A}\, a_\alpha \Leftarrow x \Leftarrow b_{\beta\, \beta\in B}]) = \inf_{\alpha\in A,\, \beta\in B} ((x - a_\alpha)/(|x|+2|a_\alpha|+1), (b_\beta - x)/(|x|+2|b_\beta|+1)).$$

Then we obtain

$$r_{x>1}(x_1) = r_{x>1}(1 + 10^{-10}) = (1 - R_{x>1}(1 + 10^{-10}))/2 =$$
$$(1 - 10^{-10}/(2 + 10^{-10}))/2 = 1/(2 + 10^{-10})$$

a little smaller than 1/2 and

$$r_{x>1}(x_2) = r_{x>1}(1 + 10^{10}) = (1 - R_{x>1}(1 + 10^{10}))/2 =$$
$$(1 - 10^{10}/(2 + 10^{10}))/2 = 1/(2 + 10^{10})$$

very small, both in accordance with intuition.
Introduced risk brings (also by distributions) adequate estimations of approximation quality, exactness confidence, and reliability. The general risk theory is very effective by setting, reasonably simulating, and solving many types of problems of science, engineering, and life.
References

[1] Encyclopaedia of Mathematics. Ed. M. Hazewinkel. Volumes 1 to 10. Kluwer Academic Publishers, Dordrecht, 1988-1994
[2] Gelimson, L. G.: Elastic Mathematics. General Strength Theory. The “Collegium” All World Academy of Sciences Publishers, Munich, 2004
[3] Gelimson, L. G.: Corrections and Generalizations of the Absolute and Relative Errors. In: Review of Aeronautical Fatigue Investigations in Germany During the Period May 2005 to April 2007, (Eds.) Dalle Donne, C., Vermeer, P., CTO/IW/MS-2007-042 Technical Report, Aeronautical fatigue, ICAF2007, EADS Innovation Works Germany, 2007, 49-50

5 Fatigue and Fracture of Metallic Fuselage Materials

5.1 Crack Detection using a Contact-Free Optical Measurement Method

R. Brucksch, J. Bär, A. Schweickert and H.-J. Gudladt (UniBW München)

The evaluation of aircraft structures concerning its fatigue resistance is performed by full-scale fatigue tests. One of the main tasks during these tests is the detection of nucleated cracks and their propagation. Because of the high personnel workload for classical non-destructive evaluation (NDE) methods, the aim of this work is to investigate other contact-free optical measurement methods for crack-detection applicability.

Experimental Procedure
For this experimental study the high-strength and high fracture-toughness aluminium alloy EN AW 7475-T761 (clad) was used. Centre-cracked-tension (CCT) specimens were made of 2.88mm thick plates of this alloy.
For crack detection as well as crack extension measurement the direct current potential drop method (DCPD) was used. In order to minimize the influence of temperature on the DCPD measurement, a special test chamber has been developed.
With this test-setup it was possible to create a defined damage situation in the specimen which reflects in the crack length as the basis for the following optical detection procedure.
For this research the measurement system Q-400 for optical image correlation (Grey-Scale-Correlation-Method) by Dantec Dynamics [1] was tested. At first, the system had to be calibrated by using a checkerboard pattern in the plane of interest. The latter could be areas of high damage accumulation, denoted as hot spots for fatigue testing. Prior to the test, different patterns with pronounced light/dark contrast were painted on the specimen surface. As a reference, a first picture was taken without external load. Next, a fatigue crack was created by using a servo hydraulic test rig. After a couple of cycles the rig was forced to establish a constant tension load on the specimen and a second picture was taken. With the analysis software Istra4D, using the cross-correlation-function, it is possible to measure the in-plane displacement field, obtained from the first and the second picture. This procedure has been undertaken during the whole fatigue test.

Results
By using the Grey-Scale-Correlation-Method it was possible to detect cracks with a length of 1mm in minimum in the vicinity of the centre hole (Figure 5.1). Further, one can find a fit-function for that specimen geometry to correlate the virtual notch factor (calculated peak-stress over external load) with the crack-length. Hence, the tested procedure is applicable for detection of the crack and its propagation.

One of the main difficulties is the placement of an adequate spot pattern on the specimen surface. The quality of the crack measurement is strongly dependent on this kind of pattern. To achieve good results there should be no agglomerations of spots with different sizes. Furthermore, it is very difficult to produce a fine spot structure next to edges and holes. However, the latter is of main importance for crack-detection in lightweight structures. As a first result, it has been found that the best way to produce spots with good width and low standard deviation, even in the vicinity of a hole, was the use of a permanent pen on a white primer (Figure 5.2).

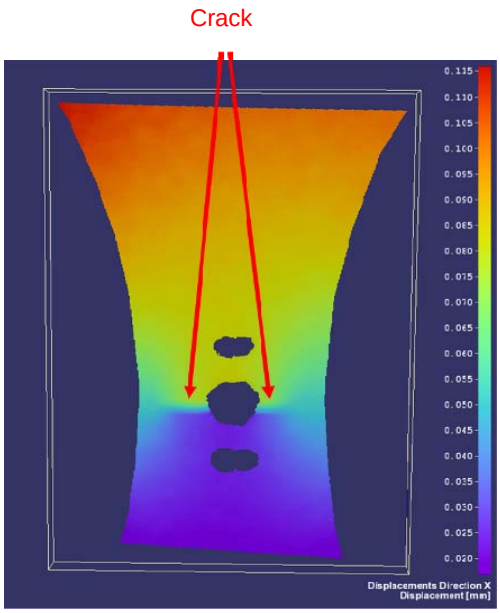

Figure 5.1 Displacement Field of a damaged CCT-specimen

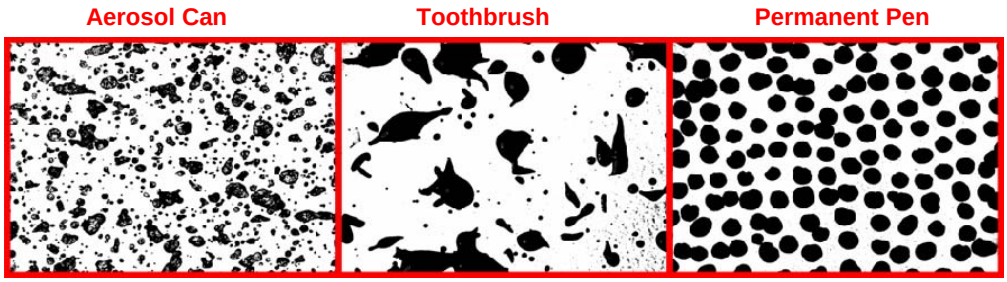

Figure 5.2 Different methods for placing high-contrast spots on the specimen surface

Conclusion

The tested image correlation system was applicable for crack detection and detection of crack propagation. The main advantage of the system is its portability and the fact, that it is contact-free. At first, it needs to be calibrated with a special checkerboard pattern in the plane of interest. Thereafter, the experiment has to be moved after this calibration procedure. Secondly, one needs a high-contrast spot pattern on the specimen surface, which is another bottleneck of this measurement method. To improve the measurement one should use a marking laser for enhancement of the spot pattern reproducibility.

Furthermore one can use the method only on visible planes of the structure. Therefore, it seems to be a good system for damage detection in laboratory scale, but it is not easily applicable for full-scale-fatigue tests.

Reference

[1] www.dantecdynamics.com (11.02.2009)

5.2 Laser Shock Peening to Improve the Fatigue Resistance of Highly Stressed Structural Components

E. Hombergsmeier (EADS-IW) and D. Furfari (Airbus)

Laser shock peening (LSP) is a mechanical process capable to introduce compressive residual stresses into the surface of a metallic component. The residual compressive stress field can extend deeper below the treated surface than that produced by conventional shot peening (i.e. with steel balls). The effect of such deep compressive stress profile results in a significantly greater benefit in fatigue resistance after laser shock peening compared to shot peening.

LSP

Metal Improvement Company (MIC) developed its laser peening process (Figure 5.3) in conjunction with the Lawrence Livermore National Laboratory. LSP imparts a layer of beneficial residual compressive stress underneath the surface of metal components to help them better resist the detrimental effects of fatigue. This process has tremendous potential for the mitigation of otherwise life-limiting surface cracking, especially if applied to the airframe at critical locations where the conventional methods (e.g. shot peening) would have very limited benefit. This has obvious benefits for extending the service life of metallic components at the manufacturing stage but it may also be possible to apply this technique to in-service aircraft to extend the service goals of existing structures. Degradation processes, such as fatigue, limit service lives of aircraft structures. Technologies and methodologies that improve the resistance of structures to these degradation processes are of benefit to industry in terms of extending the service life of the structure and reducing maintenance costs. In addition to the improvement of the manufacturing methods, which would directly impact on quality improvement and cost reduction, it is necessary to investigate these technologies in view of increasing operational costs, for example, extending maintenance intervals by enhancing metals performance.

The laser peening process is applicable to a range of aerospace alloys (Ti, AL or Steel) and this programme aims to understand benefits (improved fatigue life) of applying the LSP process to typical airframe structures made of high strength Al alloy (7xxx series) with “heavy” gauges (i.e. thickness greater than 30 mm). It is therefore essential and a challenge to investigate the influence of engineered residual stresses on metallic materials used in aircraft structures (e.g. Aluminium alloys).

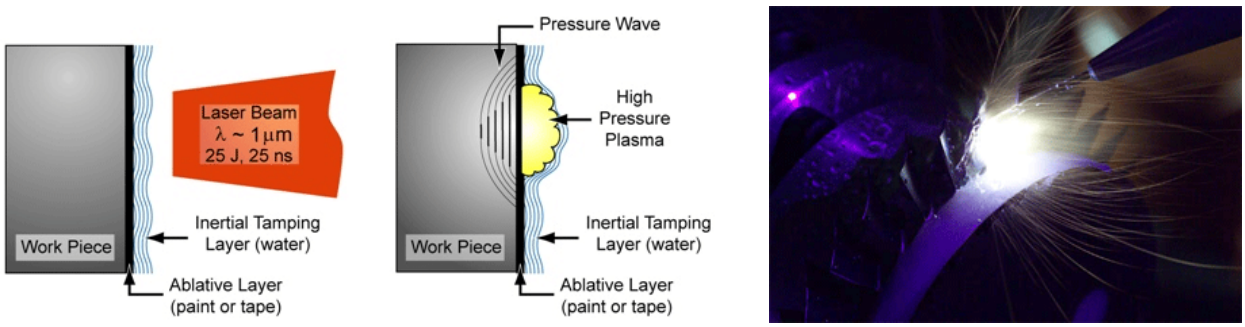

Figure 5.3 Sketch and photograph of Laser shock peening process at MIC

Fatigue improvement

First fatigue investigations are performed on notched specimens made of 7xxx aluminium plate material. For comparison the specimens are tested in milled condition, shot peened according to Airbus specification and laser shock peened by MIC in UK.

Due to superposition of compressive residual stresses onto the tensile stresses generated during cyclic fatigue, crack propagation is suppressed if the net stresses remain in the compressive state. Therefore a significant improvement of the fatigue life was found for an R ratio of 0.1. Shot peening leads to a fatigue improvement of about 15 % for the specimens shown in fig. y. For the same specimen geometry a fatigue life improvement of about 25 to 35 %, depending on the load level, can be obtained after laser shock peening (Figure 5.4). However not only for the positive R ratio, where it is quite obvious, but also for the negative R ratios, R = -1 and -3 a similar increase of the fatigue life is generated by shot peening and laser shock peening (Figure 5.4). This positive effect of the laser shock peening treatment on the fatigue behaviour can be explained by the much deeper residual stress profile in comparison to shot peening (Figure 5.5), created by the LSP process.

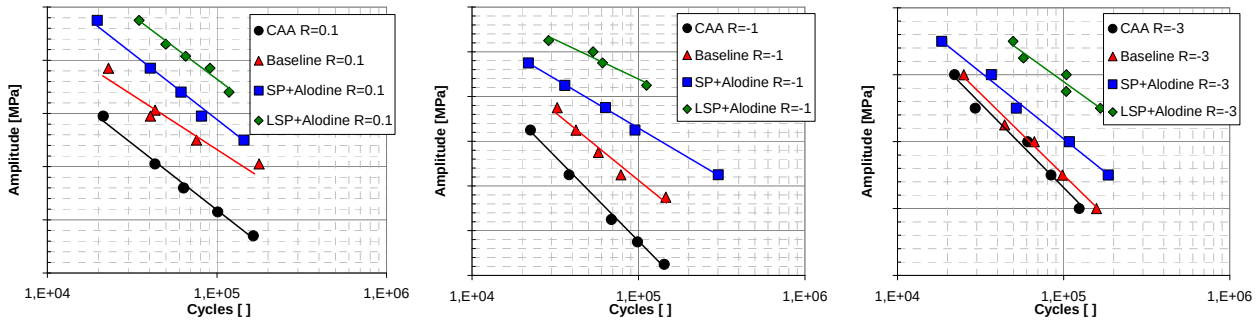

a) R ratio 0.1 b) R ratio -1 c) R ratio -3

Figure 5.4 Fatigue test results of anodized, milled, shot peened and laser shock peened notched specimens

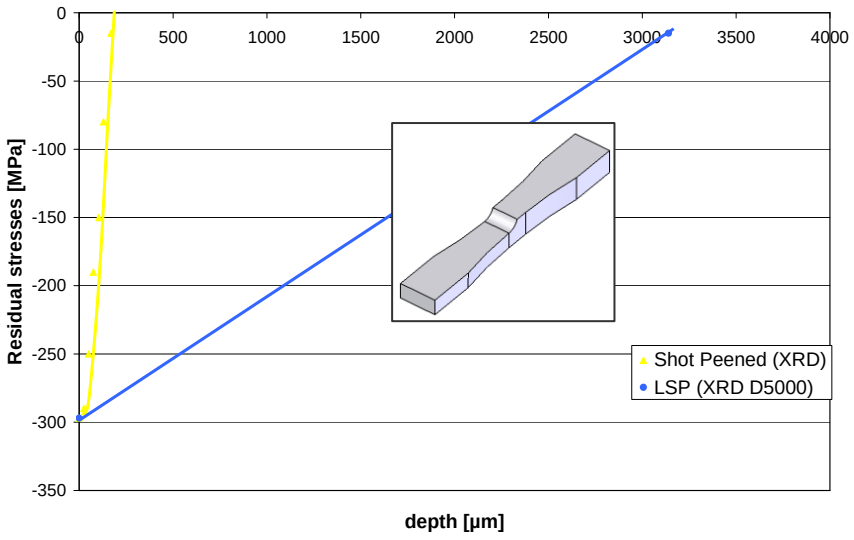

Figure 5.5 Residual stress profile of shot peened and laser shock peened fatigue specimens

5.3 Linear Combination Method in Three-Dimensional Elasticity

L.G. Gelimson (IFST)

In engineering, including aeronautical fatigue, it is often necessary to optimize structural elements via analytic methods [1-4] (along with FEM). Let us consider a general problem (an arbitrary set of functional equations) which perhaps can be represented in the form

$$F_\alpha[_{\beta\in B}\, f_\beta[_{\gamma\in\Gamma} z_\gamma]]\; r_\alpha\; 0\; (\alpha\in A)$$

where

F_α are known functions ($\alpha\in A$);
f_β are desired functions ($\beta\in B$);
z_γ are independent variables ($\gamma\in\Gamma$);
A, B, Γ are corresponding sets of indexes;
$[_{\alpha\in A}\, a_\alpha]$ is a system of indexed elements, a_α, in particular:
$[_{\beta\in B}\, f_\beta]$ is a system of indexed desired functions,
$[_{\gamma\in\Gamma}\, z_\gamma]$ is a system of indexed independent variables;
r_α is a general relation.

The essence of the linear combination method is that each known function, F_α, and each desired one, f_β, is represented as a finite or infinite linear combination of functions from a chosen linearly independent class. It is closed over all the known functions, F_α, external with respect to the desired functions, f_β. The combination factors are numbers determinate for the known functions, F_α, and indeterminate for the desired functions, f_β. Then the equations of the set become linear algebraic over the indeterminate factors and are used to obtain their values.
In particular, to the homogeneous harmonic equation

$$\nabla^2\varphi(x, y, z) = 0$$

over desired function $\varphi(x, y, z)$ in the Cartesian coordinates, x, y, z, in the class of power functions (power series), (or, equivalently, in a general *pseudosolution* [2]

$$L(r, z) = \sum_{i=0}^{\infty}\sum_{j=0}^{\infty}\sum_{k=0}^{\infty} a_{ijk}x^i y^j z^k),$$

the linear combination method made it possible, to determine the most general solution

$$\varphi(x, y, z) = \sum_{i=0}^{\infty}\sum_{j=0}^{\infty}\sum_{k=0}^{\infty} (-1)^{[i/2]}\,[i/2]!(i!j!k!)^{-1}$$
$$\sum_{l=0}^{[i/2]} (j + 2l)!(k + 2[i/2] - 2l)!\,(l!\,([i/2] - l)!)^{-1}$$
$$a_{i - 2[i/2],\, j + 2l,\, k + 2[i/2] - 2l}\; x^i y^j z^k$$

where

$$[m] = \text{entier } m$$

is the integral part of a real number m, a_{0jk} and a_{1jk} are two arbitrary number sequences,

$$0 \le j < \infty,\; 0 \le k < \infty.$$

To the homogeneous biharmonic equation

$$\nabla^2\nabla^2 L(r, z) = 0$$

over desired function $L(r, z)$ in the cylindrical coordinates, r, z, in the class of power functions (power series) (or, equivalently, in a general *pseudosolution* [2]

$$L(r, z) = \sum_{i=0}^{\infty}\sum_{j=0}^{\infty} a_{ij}r^{2i}z^j),$$

the same method allows determining the most general solution

$$L(r, z) = \sum_{i=0}^{\infty}\sum_{j=0}^{\infty} (-1)^{i+1} i!^{-2} j!^{-1}[(2i + j - 2)!i\,2^{2-2i}a_{1,\,2i+j-2} + (2i + j)!(i - 1)2^{-2i}a_{0,\,2i+j}]r^{2i}z^j$$

where by $k < 0$ we conventionally consider

$$k! = 1,$$

$$a_{1k} = 0,$$

a_{0j} and a_{1j} are two arbitrary number sequences,

$$0 \le j < \infty.$$

The both general solutions lead to the power modification of an analytic macroelement method (AMEM) [2-4] very suitable for three-dimensional problems in mechanics, strength, and fatigue [1-4].

References

[1] Handbuch Struktur-Berechnung. Prof. Dr.-Ing. L. Schwarmann. Industrie-Ausschuss-Struktur-Berechnungsunterlagen, Bremen, 1998

[2] Gelimson, L. G.: Elastic Mathematics. General Strength Theory. The “Collegium” All World Academy of Sciences Publishers, Munich, 2004

[3] Gelimson, L. G.: Providing Helicopter Fatigue Strength: Flight Conditions. In: Structural Integrity of Advanced Aircraft and Life Extension for Current Fleets – Lessons Learned in 50 Years After the Comet Accidents, Proceedings of the 23rd ICAF Symposium, Dalle Donne, C. (Ed.), 2005, Hamburg, Vol. II, 405-416

[4] Gelimson, L. G.: Theory of Measuring Stress Concentration. In: Review of Aeronautical Fatigue Investigations in Germany During the Period May 2005 to April 2007, (Eds.) Dalle Donne, C. and Vermeer, P., CTO/IW/MS-2007-042 Technical Report, Aeronautical fatigue, ICAF2007, EADS Innovation Works Germany, 2007, 53-54

5.4 Analytic Macroelement Method in Axially Symmetric Elasticity

L.G. Gelimson (IFST)

To optimize structural elements in engineering including aeronautical fatigue, analytic methods [1-5] (along with the finite element method) are used.

An analytic macroelement method (AMEM) has been created in two modifications obtained via a linear combination method and a partial method (all by the author [4, 5]). They have been applied, e.g., to solving equations and their sets in axially symmetric elasticity by piecewise smooth boundary conditions.

The essence of the power modification of the AMEM is that the obtained general power representation of the Love’s axially symmetric biharmonic stress function [2]

$$L(r, z) = \sum_{i=0}^{\infty} \sum_{j=0}^{\infty} (-1)^{i+1} i!^{-2} j!^{-1} [(2i + j - 2)! i \, 2^{2-2i} a_{1,\, 2i+j-2} + (2i + j)!(i - 1) 2^{-2i} a_{0,\, 2i+j}] r^{2i} z^{j},$$

where by $k < 0$ we conventionally consider $k! = 1$ and $a_{1k} = 0$,

a_{0j} and a_{1j} being two arbitrary number sequences, $0 \le j < \infty$,

is used by steps to exactly or approximately satisfy the boundary conditions in a problem to be solved. The displacements and stresses are determined via applying the Love’s linear differential operators [2] to L. Love has shown that the biharmonicity of L is sufficient for precisely satisfying all the equilibrium and continuity equations. The biharmonicity necessity problem is now set and positively solved. For a cylindrical body, it is shown that it is enough to consider one base to be free of loads. The power expansions of the nonzero boundary conditions lead to four infinite subsets of linear algebraic equations over the coefficients in the function L. Their general solutions by their homogeneity are linearly expressed through the sequential zeroes of two Bessel functions and two ones analogous to them. It is shown that the compatibility of the boundary conditions in a boundary-value problem is necessary and sufficient for its exact solvability. If the body has a complicated form or the conditions are discontinuous then the body is mentally cut with canonical surfaces to a few macroelements. Solutions for them are conjugated by minimiz-

ing the responsible mean square residuals, collocation ones, and minimax modulus residuals. Their linear or quadratic correction makes stress determination in a strength problem more precise. For the Lamé solution [1], it is shown that the known linear generalization is the unique exact one.

The integral modification of the AMEM in axially symmetric elasticity is obtained by applying the partial method to the set of the differential equations in elastic stresses. The both equilibrium equations together with the continuity one having the first order allow precisely expressing the normal stresses via the boundary conditions in stresses and the distribution of the shear stress. The remaining continuity equation integro-differential of the second order makes exactly solving it unreal. Instead of that, by the introduced principle of tolerable simplicity [4], for the shear stress $\tau(r, z)$, its simplest statically possible distribution ensuring the equilibrium of each body part cut off by an arbitrary coaxial cylindrical surface is determined. For a cylindrical body $a \le r \le b$, $c \le z \le d$, we have

$$\tau(r, z) = (b^2 - r^2)(b^2 - a^2)^{-1}\tau(a, z) + (r^2 - a^2)(b^2 - a^2)^{-1}\tau(b, z) + 6(z - c)(d - z)(d - c)^{-3}$$
$$\{-(b^2 - r^2)(b^2 - a^2)^{-1}\int_c^d \tau(a, z')\,dz' + (b/r - (r^2 - a^2)(b^2 - a^2)^{-1})\int_c^d \tau(b, z')\,dz' +$$
$$r^{-1}\int_r^b [\sigma_z(r', d) - \sigma_z(r', c)]\,r'dr'\} + (d - z)(2c + d - 3z)(d - c)^{-2}[\tau(r, c) -$$
$$(b^2 - r^2)(b^2 - a^2)^{-1}\tau(a, c) - (r^2 - a^2)(b^2 - a^2)^{-1}\tau(b, c)] +$$
$$(z - c)(3z - c - 2d)(d - c)^{-2}[\tau(r, d) - (b^2 - r^2)(b^2 - a^2)^{-1}\tau(a, d) - (r^2 - a^2)(b^2 - a^2)^{-1}\tau(b, d)].$$

The radial, tangential, and axial normal stresses are determined by the formulae

$$\sigma_r(r, z) = (a/r)^2(b^2 - r^2)(b^2 - a^2)^{-1}\sigma_r(a, z) + (b/r)^2(r^2 - a^2)(b^2 - a^2)^{-1}\sigma_r(b, z) +$$
$$\mu r^{-2}\int_a^r \sigma_z(r', d)r'dr' - \mu r^{-2}(r^2 - a^2)(b^2 - a^2)^{-1}\int_a^b \sigma_z(r', d)r'dr' - 2^{-1}(1 + \mu)\int_a^r(\partial\tau(r', z)/\partial z)dr' +$$
$$2^{-1}(1 + \mu)\,b^2r^{-2}(r^2 - a^2)(b^2 - a^2)^{-1}\int_a^b(\partial\tau(r', z)/\partial z)dr' - 2^{-1}(1 - \mu)r^{-2}\int_a^r(\partial\tau(r', z)/\partial z)(r')^2dr' +$$
$$2^{-1}(1 - \mu)r^{-2}(r^2 - a^2)(b^2 - a^2)^{-1}\int_a^b(\partial\tau(r', z)/\partial z)(r')^2dr' + \mu r^{-1}\int_z^d \tau(r, z')dz' -$$
$$\mu a r^{-2}(b^2 - r^2)(b^2 - a^2)^{-1}\int_z^d \tau(a, z')dz' - \mu b r^{-2}(r^2 - a^2)(b^2 - a^2)^{-1}\int_z^d \tau(b, z')dz' \ (\mu \text{ the Poisson ratio});$$
$$\sigma_t(r, z) = \partial(r\sigma_r(r, z))/\partial r + \partial(r\tau(r, z))/\partial z;$$
$$\sigma_z(r, z) = \sigma_z(r, d) + r^{-1}\int_z^d(\partial(r\tau(r, z))/\partial r)dz'$$

with exact or approximate generalization of the Lamé solution [1]. To estimate the accuracy, the obtained solution is substituted into the remaining equation. For its left side in the body domain, the mean value is divided by the least upper bound on the sum of the moduli of its algebraic summands, each of them being a product of functions of the initial data.

References

[1] Lamé, G.: Lecons sur la theorie mathematique de l'élasticite des corps solides. Gauthier-Villars, Paris, 1852

[2] Love, A. E. H.: A Treatise on the Mathematical Theory of Elasticity. Vols. I, II. Cambridge University Press, Cambridge, 1892, 1893

[3] Handbuch Struktur-Berechnung. Prof. Dr.-Ing. L. Schwarmann. Industrie-Ausschuss-Struktur-Berechnungsunterlagen, Bremen, 1998

[4] Gelimson, L. G.: Elastic Mathematics. General Strength Theory. The "Collegium" All World Academy of Sciences Publishers, Munich, 2004

[5] Gelimson, L. G.: Discretization Errors by Determining Area, Volume, and Mass Moments of Inertia. In: Review of Aeronautical Fatigue Investigations in Germany During the Period May 2005 to April 2007, (Eds.) Dalle Donne, C., Vermeer, P., CTO/IW/MS-2007-042 Technical Report, Aeronautical fatigue, ICAF2007, EADS Innovation Works Germany, 2007, 20-22

6 Fatigue and Fracture of Composites

6.1 Damage Behaviour of Hybrid Titanium-PEEK /AS4 Composite Laminates in Mixed Mode Bending – Experiments and Numerical Simulations

P. Naghipour, J. Schneider, L. Chernova, M. Bartsch, J. Hausmann and H. Voggenreiter (DLR)

Hybrid laminate architectures composed of carbon fibre reinforced plastic plies (CFRP) with alternating titanium foils combine advantages of metals and composites, utilizing the possibility of manufacturing anisotropic properties on demand, such as high specific stiffness and strength, and high impact tolerance.

Fibre reinforced composites often exhibit complex failure mechanisms as an interaction of intralaminar damage modes such as matrix cracking and fibre rupture and interlaminar damage modes, predominantly delamination. Interfacial cracking between layers or delamination can be a result of impact, bearing load in bonded joints, or any other source of significant interlaminar stress. In order to simulate the mixed mode damage mechanism of Ti/CFRP laminates, it is essential to develop the correct damage model of each of the constituents, especially the CFRP. As various factors such as fibre orientations, different stacking sequences, and combination of inter- and intralaminar damage modes might affect the damage mechanism in CFRP, more complexity is involved in the mechanical behaviour of this constituent of the hybrid laminate. Hence, the ongoing work focuses at first on the analysis of the mixed mode damage in the CFRP part.
The test specimens are 24–ply polymer matrix composites with thermoplastic PolyEther Ether Ketone (PEEK) as the matrix material and 60% volume fraction of AS4 carbon fibres. Some known advantages of the thermoplastic polymers such as their resistance to higher temperatures, good formability by reheating and weldability, environmentally friendly processing, and their certification for use in aeronautics were among the main reasons to prefer them to a thermoset matrix material. Each laminate is 25 mm wide, 150 mm long, and 3.12 mm thick, and a non adhesive ply, inserted before consolidation, is used as the delamination plane.

The mixed mode bending (MMB) experiment, first introduced by Crews and Reeder [1], provides the possibility to combine the influence of normal (mode I) and shear or sliding stresses (mode II) on interlaminar delamination using a single test apparatus. The MMB loading was represented by a superposition of pure mode I and mode II loadings, conducted by a single load P. Figure 6.1 shows the MMB loading facility.

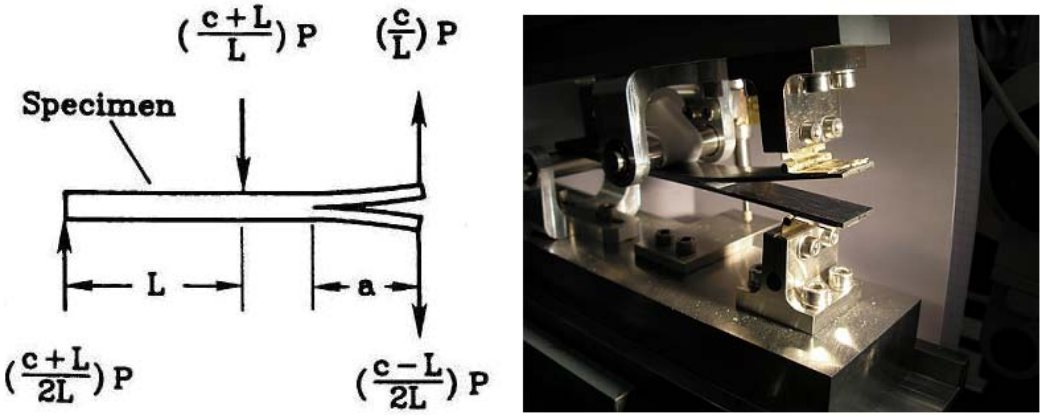

Figure 6.1 MMB test apparatus and schematic loading description after [1]

The numerical model created in ABAQUS [2] consists of individual damageable plies to capture any in-ply damage and interface elements in between them. The in-ply damage in each lamina is described by the built-in Hashin damage model in ABAQUS [2]. Each ply is defined as orthotropic material in plane stress. Damage initiation, which refers to the beginning of degradation of the ply response, is due to four main failure criteria, namely: fibre ruptures in tension, fibre buckling in compression, matrix cracking under transverse tension and shear, and matrix crushing under transverse compression. Damage propagates when the total fracture energy in any of the four mentioned cases reaches its maximum value (G_{cmax}), specified by the user as an input parameter. After damage initiation, three independent non-negative in-ply damage parameters, d_f, d_m, and d_s reduce the ply stiffness numerically in fibre, transverse, and shear directions, respectively, until the final failure point is reached. The cohesive zone approach is adopted to describe interface finite elements between the plies, incorporating a cohesive mixed-mode damage model. Zero thickness 8 node cohesive elements, implemented as a user defined element (UEL) in ABAQUS, are mainly based on the constitutive model suggested by Davila et al [3].

The parameter for the numerical model were taken from experimentally achieved material data, either from literature or own mechanical experiments. The results from virtual and laboratory MMB-experiments have been compared. Figure 6.2a displays the results for unidirectional (UD) laminates for different mode mixtures and Figure 6.2b for different stacking sequences of multi-directional (MD) lay ups for the same mode mixture of m=50%.

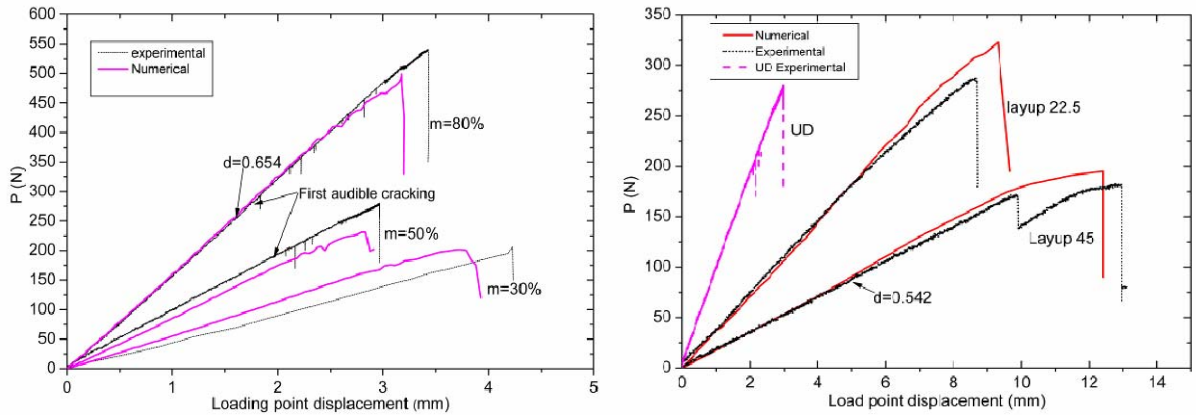

a) **b)**

Figure 6.2 Comparison between simulation and experiment of MMB test for a) UD-laminates with different mode mixtures and b) different MD lay ups for 50% mode mixture

It is generally observed that fibre angle orientation and stacking sequences have a global effect on load-displacement response. The in situ effects in MD laminates are characterized by higher transverse tensile and shear strengths of a ply when it is constrained by plies with different fibre orientations in a laminate, compared with the strength of the same ply in a unidirectional laminate [4].

Experimental and numerical results have been achieved for quasi-static loading in MMB. The material behaviour for cyclic loading in MMB will be investigated in the ongoing work.

References

[1] J.H. Crews, J.R. Reeder (1988) A mixed-mode bending apparatus for delamination testing: NASA TM 100662.

[2] Hibbitt, Karlsson, and Sorensen (2006) ABAQUS 6.6 User's Manuals, Pawtucket, U.S.A.
[3] C.G. Davila, P.P. Camanho PP, M.F.S.F. de Moura (2001), Mixed-Mode decohesion elements for analyses of progressive delamination. In: Proceedings of the 42nd AIAA/ASME/ASCE/AHS/ASC structures. Structural dynamics and materials conference, Seattle, Washington; April 16–19, 2001.
[4] G.J. Dvorak, N. Laws, J Composite Materials. 21 (1987) 309–329.

6.2 Hybrid Structures for Concentrated Load Transmission in Fibre Composites: Initial Experiments

P. Vermeer (EADS-IW), R.C. Alderliesten and Rinze Benedictus (TUDelft)

The current generation aircraft in development consist of +50% (carbon) fibre composites as these materials couple a low density with extremely high directional strength and stiffness. Additionally, fibrous composites perfectly allow in-plane properties to be freely specified; generally by variation of fibre type, orientation and lay-up, so also a quasi-isotropic state can be obtained. However, a concentrated transmission of load strikes on inherent violations of the composite's basic design; structural coupling by conventional mechanical fastening provokes the composite's notch sensitivity, its low shear and bearing strengths and the critical dependence on the laminate lay-up. Although increasing the (quasi-isotropic) joint thickness would make the design uncritical to bearing failure, this is in conflict with the aspiration to structural efficiency. In addition unfavourable effects and increasing complexity are often induced.

As fibre metal laminates (FML) are known to be suitable for mechanical fastening, adopting the concept of FML seems to be an elegant solution for optimising the joining area of carbon fibre reinforced polymer (CFRP) structures. Hence, a local (inverted) hybrid titanium composite laminate (HTCL) is created by insertion of thin titanium foils in the CFRP laminate, replacing those fibre layers whose orientation is contributing least to load transfer [1] (Figure 6.3).

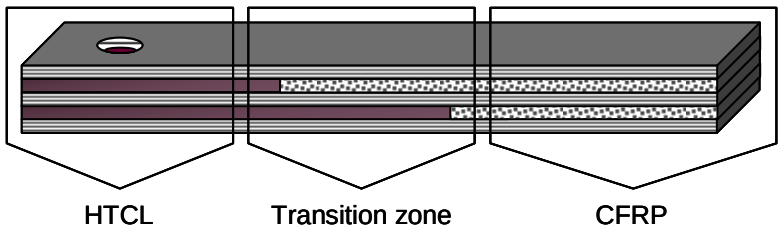

Figure 6.3 Schematic lay-up of a hybrid laminate with its corresponding areas HTCL (2×Ti / 3×CFRP) with hole, Transition zone and CFRP (0°/90°)

This requires investigation of the transition zone from the CFRP laminate into the hybrid area and the behaviour of the HTCL under fatigue loading. The latter has a correlation to previous studies on FML for fuselage applications, and it is likely that the different constituents in HTCL affect the laminate's mechanical behaviour.
This study can be considered as an element of advanced hybrid structural concepts in composite aircraft design, supporting the development of HTCL and its transition region for local–reinforced / fastening–optimised CFRP structures. Focus is on similarities with existing FML, model adaptation and experimental validation.

Investigations on fatigue crack initiation and propagation in HTCL show promising intermediate results; it has been confirmed that fibres generally have no positive effect on the fatigue crack initiation life causing the introduction of significant (tensile) curing stresses (Figure 6.4), increasing the actual stress level in metallic layers and therewith result in early initiation of cracks. The modified classical laminate theory (CLT) is a reliable and valid calculation method for residual stress calculation as initial experiments show a good correlation with the CLT results [2].

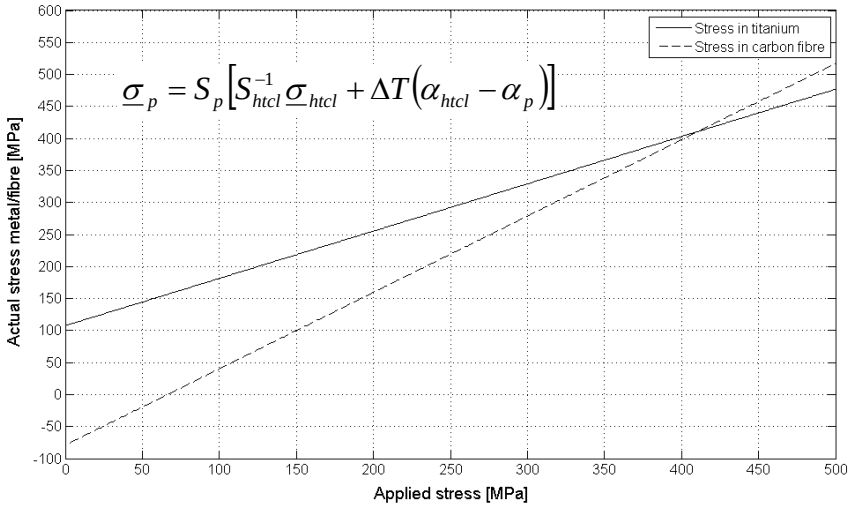

Figure 6.4 Actual stresses in metal and fibre layers due to curing and additional applied stresses. Intersection at 411MPa

The mechanisms seem qualitatively similar to Glare, as crack propagation does occur in hybrid titanium composite laminates featuring a fibre/crack bridging effect but without affecting or damaging the fibres. The occurrence of FML-typical delamination in an area around the crack is considered to be present, however, due to the applied experimental methods of X-ray computer tomography not resolvable (Figure 6.5). Hence, the visualisation of delamination and in-situ techniques for measurement of crack lengths remain special points of attention.

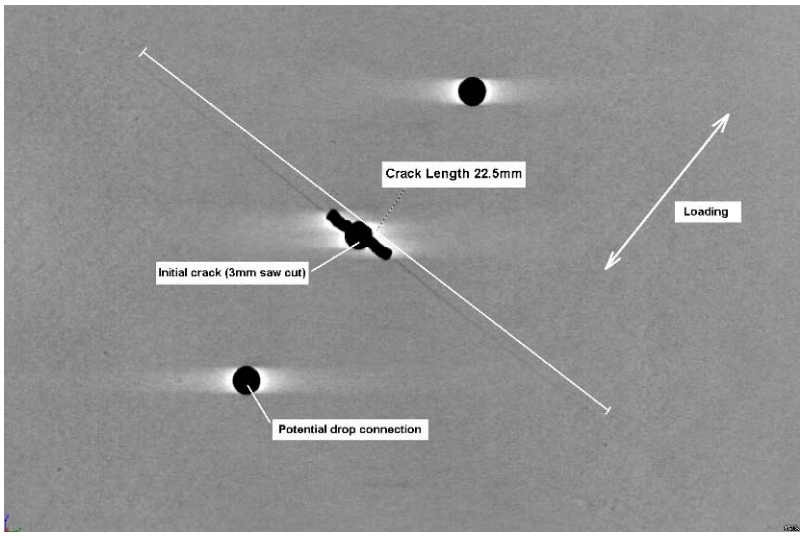

Figure 6.5 HTCL–2/3 fatigue crack propagation specimen.

The near future focus will be on enhancement of the experimental techniques by testing with specific equipment and methods, e.g. digital image correlation, as Rodi et al. [3] proved this to be very suitable for investigating delamination in FML with an inverted lay-up.

References

[1] Kolesnikov, B., Herrmann, A. and Pabsch, A. (1999), WO 00/56541.
[2] Homan, J.J. (2006), *Int. Journal of Fatigue*, vol. 28, pp. 366–374.
[3] Rodi, R., Alderliesten, R.C. and Benedictus, R. (2009), In: *Bridging the Gap between Theory and Operational Practice*, Proceedings of the 25th ICAF Symposium, Rotterdam.

6.3 Fatigue Crack Growth in CFRP Foam-Core Sandwich Structures

M. Rinker, M. John and R. Schäuble (Fraunhofer)

Sandwich structures offer a good ratio of bending stiffness and strength to weight. The application of carbon fibre reinforced polymers for the face sheets in combination with lightweight core materials provide potential for optimization. Using closed cell foams complex core preforms can be manufactured; therefore it is possible to produce high integral sandwich components. These can especially be used in structures which have a high ratio of strength and stiffness to weight and are at risk to fail by buckling. Hence those sandwich structures qualify for application in planes for commercial aircrafts [1]. A typical sandwich failure mode is the occurrence of cracks in the interface between face sheet and core caused by impact [2]. In the last resort the impact damage is non visible and propagates in service under cyclic loads up to global failure [3].
Quasi-static and cyclic modified DCB and ENF [4] tests (Figure 6.6 and Figure 6.7) were run to investigate the crack propagation under global Mode I and Mode II load, whereas the crack front always is under mixed mode loading due to the interface characteristics. The energy release rates were calculated using the virtual crack closure technique [5] which was applied on three dimensional finite element models of the DCB and the ENF specimens. The crack lengths in the cyclic tests were determined using a compliance method [6]. Therefore the stiffness was measured for various defined crack lengths and compared with the FE-model stiffness. Finally the Paris law was used to describe the fatigue crack propagation.

Figure 6.6 Modified DCB-Test

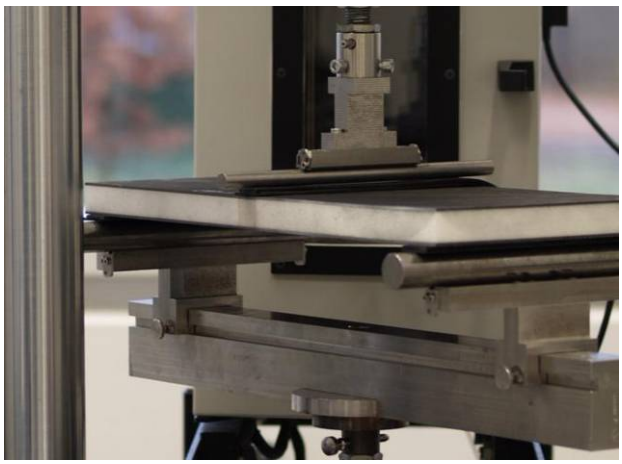

Figure 6.7 Modified ENF-Test

The specimens were manufactured by *CTC Stade* (ENF) and *EADS MAS* (DCB) using Liquid Composite Moulding technologies. The Specimens are composed of two NCF CFRP face sheets with 18 unidirectional layers (66/33/0) sandwiched with the closed cell PMI foam as core material.
Already the quasi-static tests show the repetitious material and manufacturing quality. The fracture load and the critical energy release rate were determined with small derivations (Figure 6.8). Based on the quasi-static tests the fatigue tests were run with a load ratio 0.1 and a maximum load of 60, 70, 75 and 80% of the middle static fracture load. The cyclic tests show, that crack propagation begin after many load cycles and then increases fast (Figure 6.9). The Paris-constants C and m could be determined to describe the stable crack growth under cyclic loads.

The work presented was partially funded by the *LoKosT*-Project of the *Bundesministerium für Wirtschaft und Technologie of Germany* (Federal Ministry of Economics and Technology) and realised by order of *Airbus Deutschland GmbH* and *EADS Deutschland GmbH*. The authors wish to acknowledge this support.

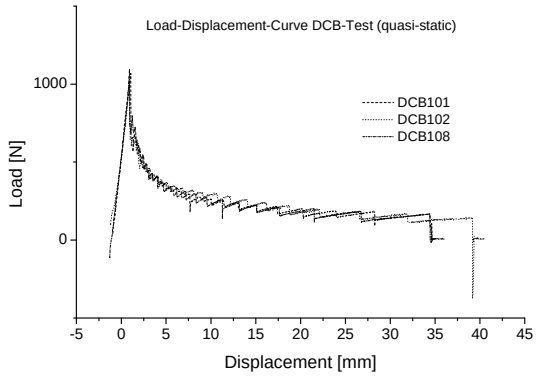

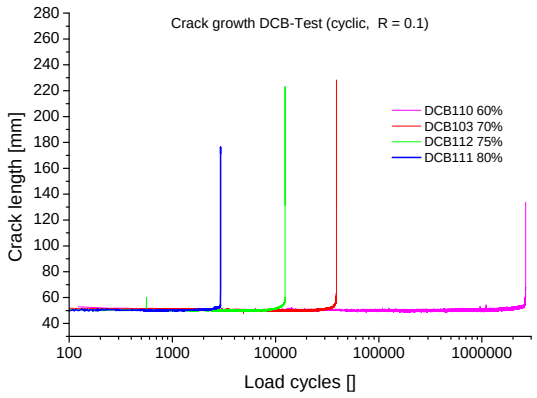

Figure 6.8 Load-Displacement-Curve quasi-static DCB-Test

Figure 6.9 Crack growth diagram

References

[1] A. S. Herrmann, P. C. Zahlen and I. Zuardy: Sandwich Structures Technology in Commercial Aviation. 7th International Conference on Sandwich Structures, Aalborg, Denmark, 2005.
[2] C. Berggreen: Damage Tolerance of Debonded Sandwich Structures. PhD thesis, Technical University of Denmark, Lyngby, Denmark 2004.
[3] Federal Aviation Administration: Damage Tolerance Assessment Handbook, U.S. Department of Transportation, 800 Independence Avenue, SW Washington, DC 20591 1993.
[4] L.A. Carlsson: On the Design of the Cracked Sandwich Beam (CSB) Specimen, Journal of Reinforced Plastics and Composites, Vol. 10, No. 4, 434-444, 1991.
[5] R. Krueger: The Virtual Crack Closure Technique: History, Approach and Applications, ICASE Report No. 2002-10, ICASE, Hampton, Virginia, USA, 2002.
[6] A. Quispitupa, C. Berggreen and L.A. Carlsson: *Fatigue Debond Growth in Sandwich Structures Loaded in Mixed Mode Bending (MMB)*, Proceedings of the 13th European Conference on Composite Materials, Stockholm, Sweden 2008.

6.4 With a "Plastic Balloon" Through the Mars Atmosphere

St. Frömmel and H.-J. Gudladt (UniBw-M)

Discovering the Mars atmosphere is a very interesting but difficult endeavour. One needs some hours during the entry phase for measuring data of interest.
Some studies describe a method to use a balloon for retarding the mars probe within the atmosphere. Completely new is the approach of the ARCHIMEDES (Aerial Robot Carrying High Resolution Imaging, a Magnetometer Experiment and Direct Environment Sensors) hypersonic-balloon project to inflate the balloon in the space outside the mars atmosphere. The balloon should have a diameter of about 10 m and operates as a parachute. In the mars atmosphere the carried instruments, e.g. a high resolution camera, a magnetometer, a thermometer, a barometer and a hygrometer should collect specific information depending from the distance to the mars surface (Figure 6.10).During the deceleration phase, the balloon-material has to resist high mechanical and thermal-induced stresses. The expected highest mission temperature reaches 200°C and the resonance frequency of the balloon should lie in the lower Hz area. In other words, the balloon must resist cyclic deformation at elevated temperatures. Consequently, most of the conventionally used polymer materials are not applicable for the mission.

Materials
Mechanical tests undertaken at elevated temperatures, similar to those expected of the mars mission, have been shown that only two materials seamed possible to use for building the balloon. The first one is named Upilex RN, a linear polyimide with aromatic ring systems in the backbone. Upilex RN is a yellow foil with 25 or 50 µm thickness. The second one is made of PBO, a linear poly benzoxazole with hetero aromatic ring systems. It is also a yellow material with a thickness of 7 µm. The chemical structure of both materials is given in Figure 6.11.

Experimental procedure
For the material selection, it is important to know the thermal stability of the polymers, used for the project and its stiffness at elevated temperatures. The thermal properties of the materials were determined with the thermo-gravimetric analysis system TGA Q500 of TA Instruments. The samples were heated from room temperature up to 800°C and 1150°C, respectively, and the loss of mass was continuously detected. For measuring the dynamic mechanical parameters the Analyzer DMA Q800 from TA Instruments was used. The samples were cut into 5 mm broad stripes between two parallel razor blades. Thereafter, these stripes were fixed in the DMA system with a film-fibre-clamp. During heating the specimen chamber linearly from 40°C to 270°C or to 400°C, the samples were cyclically deformed with a force of 1 N at a frequency of 1 Hz. During the test, stress $\sigma(t)$ elongation $\varepsilon(t)$ and the loss angle δ were measured. From these parameters, the storage modulus (E´), the loss modulus (E´´) and the loss coefficient (tan δ) have been calculated.

Results
The thermo gravimetric studies, as seen in Figure 6.12, have shown that the thermal stability of PBO is much better than for Upilex RN. PBO degrades at temperatures higher than 600°C. In contrast, for Upilex the degrading starts at 300 °C. Up to 800°C the loss of mass is about 50% and 30% for Upilex and PBO, respectively. To investigate the temperature behaviour of the mechanical properties, both, the storage as well as the loss modulus were measured by the DMA and presented in Figure 6.14. At a temperature of about 40°C the storage modulus of the 50 µm Upilex foil is close to 4 GPa. The 7 µm PBO foil, however, reaches a storage modulus higher than 48 GPa. A similar behaviour was found for the loss modulus. Going into detail, the loss modulus of the PBO shows a well pronounced peak at 262°C. In case of the PBO a peak at

about 260°C has been found. For Upilex, the loss coefficient (tan δ) is nearly almost greater than for PBO and increases rapidly up to 0.490 in a temperature range between 240°C and 270°C. This high damping ratio reflects in an accelerated creep of the material. In PBO, however, the measured damping ratio is always lower than 0.030. Consequently, the latter can be correlated with less damage, and one can expect a better creep resistance than for the Upilex (Figure 6.13).

Conclusions

Compared to other polymers, PBO shows an excellent behaviour under fatigue conditions. Unfortunately, this material is very expensive and not available for building a balloon with a diameter of 10 m. The properties of Upilex RN are not as excellent as the PBO ones, but foils of this material are easier available and the cost-value ratio is much better, too. The solution for the balloon construction seems to be a combination of both materials. The balloon should be built out of Upilex RN and the seams should be reinforced by PBO-stripes. Because of the predicted mechanical and thermal stresses during the phase of entering into the mars atmosphere it is not possible to use any adhesive. Therefore, these two materials must be welded under pressure at elevated temperatures. The verification of this method as well as the investigation of the effect of humidity and ultraviolet radiance to the mechanical characteristics of PBO are in progress.

Acknowledgements

We thank H.S. Griebel (UniBwM, chief engineer of the ARCHIMEDES mars project) for valuable discussions and for offering Upilex RN and PBO.

References

[1] E. Orndoff; Development an evaluation of polybenzoxazole fibrous structures, NASA technical memorandum 104814, 1995

[2] H.S. Griebel, B. Häusler, C. Mundt, H. Rapp, H.J. Gudladt, M. Zähringer; The hypersonic drag balloon project ARCHIMEDES – A novel atmospheric sounding probe for mars, 2008

[3] H. Griebel; Hyperschall-Ballon Projekt ARCHIMEDES – Untersuchungen über einen neuen Raumsonden Typ, Ingenieurspiegel 1/2009, 61-63, 2009

Figure 6.10 Demonstration of the AR-CHIMEDES-balloon during the flight through the outer mars atmosphere

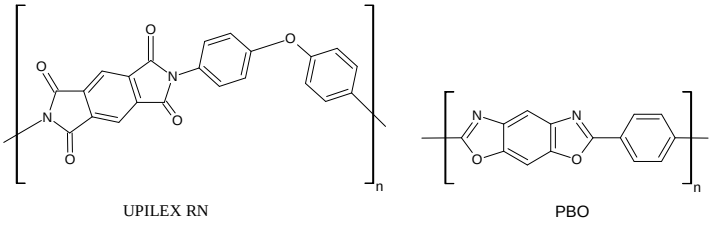

Figure 6.11 Chemical structures of the two polymers Upilex RN and PBO

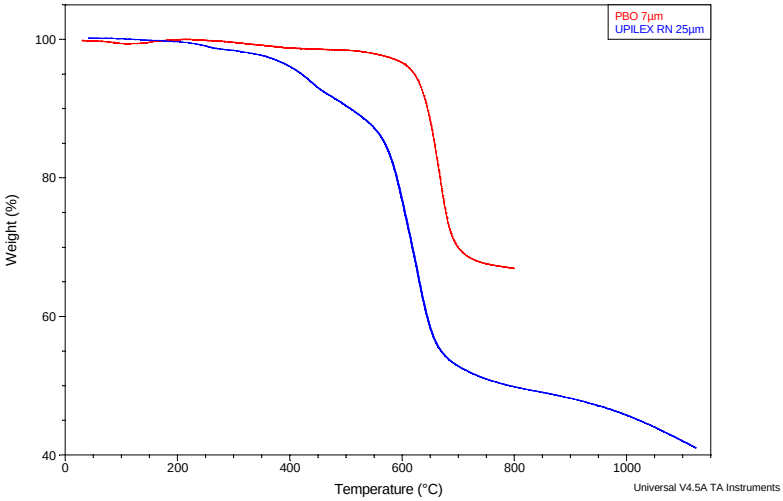

Figure 6.12 Thermo gravimetric behaviour of Upilex RN and PBO

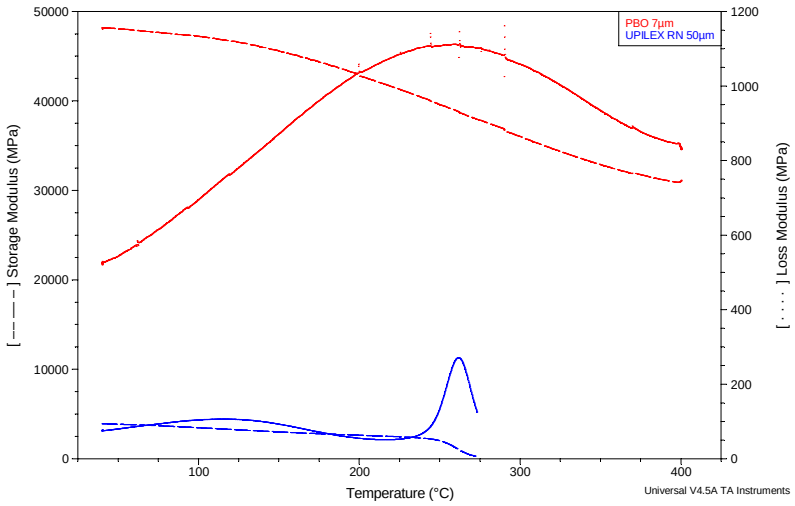

Figure 6.13 Dynamic-mechanical behaviour of Upilex RN and PBO.

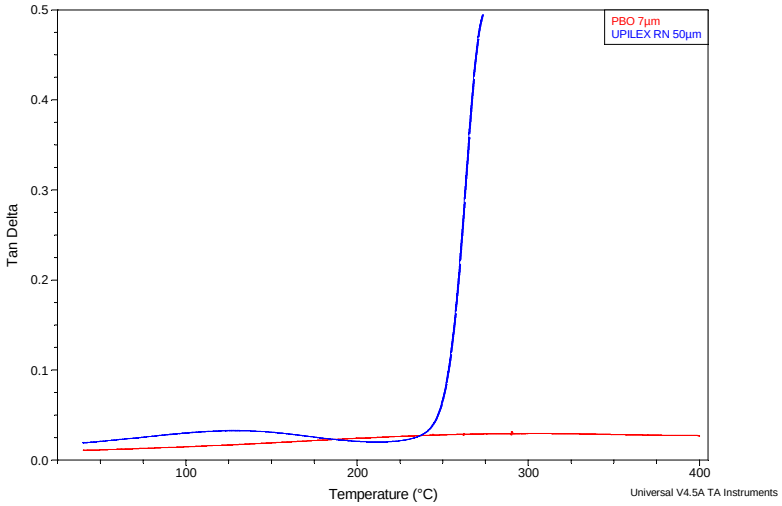

Figure 6.14 Loss coefficient tan δ of Upilex RN and PBO.

6.5 Next Generation of Composites Structures Sizing Criteria

Ll. Llopart Prieto and G. Spenninger

Due to the limited width of fabrics the manufacturing of large structures by means of cost effective infused materials like vacuum assisted process (VAP) needs dedicated splicing techniques. The EADS-MAS preferred butt joint splices may lead to resin rich areas which under static and dynamic loads results in cracking and delamination. The current design philosophy does not take into account such a damage process leading to failure. This gap has been covered by tests yielding a macroscopic factor to be applied in the stress analysis.

The industrial implementation of improved composite failure prediction tools is being evaluated and developed inside the European Aeronautic Defence & Space Company (EADS), in order to improve effectiveness in design.

To this aim EADS Military Air Systems carried out following tasks in the period 2007 to 2009:

- Completion of material data base for basic fracture mechanical parameters (*GIIc*), see Figure 6.15.
- Derivation of fast and robust analytical sizing procedures for simple non- interleaved ramps on fracture mechanical basis.
- Extension of the sizing procedure for the splice joints to cover mixed mode (peeling and shear) conditions.

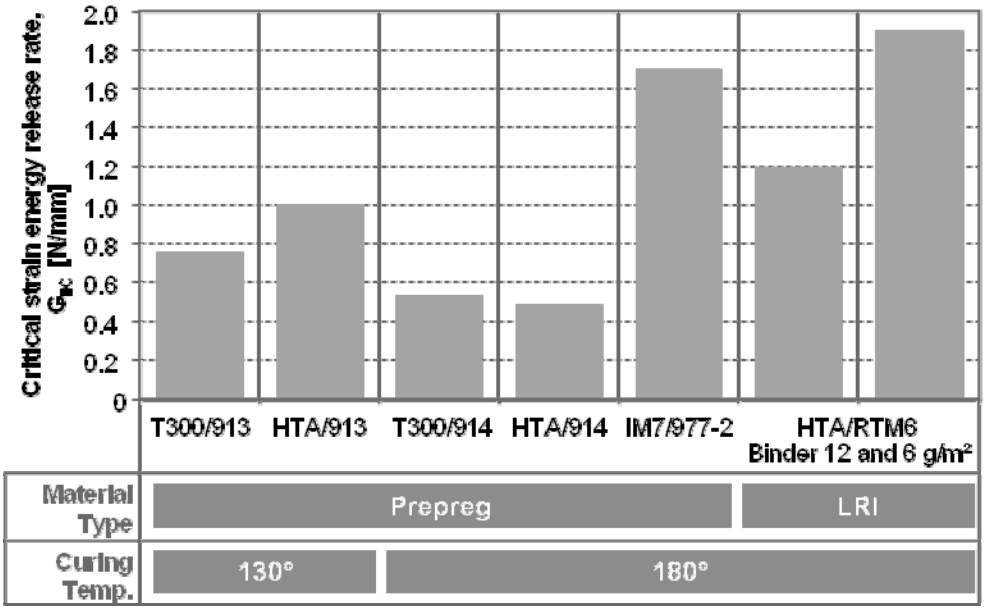

Figure 6.15 Static TCT Critical Energy Release Rate Data (Mode II)

Numerical studies and the reproduction of experimental testing for different splice configurations under Mode II loading were carried out by means of the Software StressCheck®, see Figure 6.16. Taking into account the reliable results obtained, further works are planned on spliced structures under mixed mode bending load for different composite materials. The experimental tasks as well as modelling will be carried out by Premium AEROTEC GmbH.

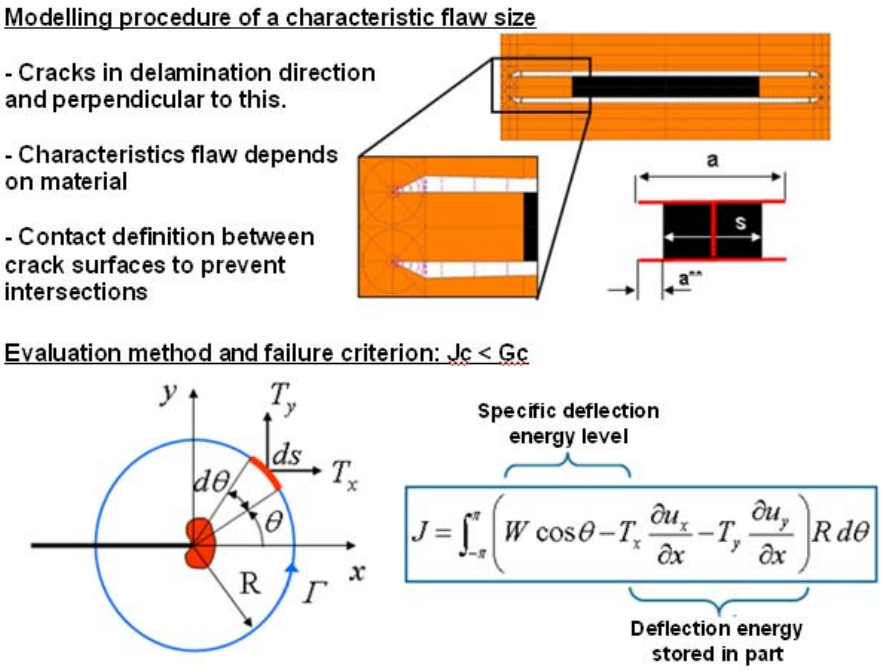

Figure 6.16 Definition of the J- Integral and its applicability in StressCheck®

6.6 Generalization of the Tresca Criterion in General Strength Theory

L.G. Gelimson (IFST)

For an isotropic ductile material with equal strength in tension and compression, the Tresca criterion (of the maximum shear stress) [1]

$$\sigma_e = \sigma_1 - \sigma_3 = \sigma_l$$

(σ_1, σ_2, σ_3 the principal stresses with

$$\sigma_1 \geq \sigma_2 \geq \sigma_3,$$

σ_e the equivalent stress, and σ_l the uniaxial limiting stress) is commonly used. This formula includes the specific value of the only material constant σ_l. Suppose this criterion to be a specific manifestation (as applied to a given material) of some unknown universal law of nature. The criterion formula itself cannot express that law, allows no generalization, and so needs a transformation. The simplest one using similarity and dimensionality theories is dividing each principal stress by the modulus σ_l of its ultimate value $\pm\sigma_l$ in uniaxlal state:

$$\sigma_1^0 = \sigma_1/\sigma_l,\ \sigma_2^0 = \sigma_2/\sigma_l,\ \sigma_3^0 = \sigma_3/\sigma_l,\ \sigma_e^0 = \sigma_e/\sigma_l.$$

The transformed criterion becomes universal:

$$\sigma_e/\sigma_l = \sigma_1/\sigma_l - \sigma_3/\sigma_l = \sigma_l/\sigma_l = 1;\ \sigma_e^0 = \sigma_1^0 - \sigma_3^0 = 1.$$

It has no evident material constant and so allows imparting a generalized sense (in comparison with this transformation) to the reduced (relative) principal stresses σ_1^0, σ_2^0, σ_3^0 according to the specific character of the strength of any given material.
For an isotropic brittle material with unequal strengths in tension and compression, it is natural to reduce each principal stress by dividing it by the modulus of its ultimate value in the corresponding uniaxial state, that is σ_t in tension and $-\sigma_c$ ($\sigma_c > 0$) in compression:

$$\sigma_j^0 = \sigma_j/\sigma_t \text{ if } \sigma_j \geq 0,\ \sigma_j^0 = \sigma_j/\sigma_c \text{ if } \sigma_j \leq 0\ (j \in \{1, 2, 3, e\}).$$

The universal criterion $\sigma_e^0 = \sigma_1^0 - \sigma_3^0 = 1$ in the space of the usual principal stresses σ_1, σ_2, σ_3

$$\sigma_e = \sigma_1 - \sigma_3 = \sigma_c\ (0 \geq \sigma_1 \geq \sigma_2 \geq \sigma 3),$$

$$\sigma e = \sigma 1 - \chi\sigma 3 = \sigma t\ (\sigma 1 \geq 0 \geq \sigma 3,\ \chi = \sigma t/\sigma c),$$

$$\sigma e = \sigma 1 - \sigma 3 = \sigma t\ (\sigma 1 \geq \sigma 2 \geq \sigma 3 \geq 0)$$

has obvious physical sense. If the signs of all the nonzero principal stresses are identical, a natural material having unequal strengths in tension and compression is similar to the two model materials. Each of them has equal moduli (either σ_t or σ_c, both instead of σ_l in the initial criterion) of the limiting stresses in tension and compression and is used when all the principal stresses are either nonnegative or nonpositive, respectively. If there are principal stresses with distinct signs, the critical states of a natural material are described by the criterion that coincides with the linear approximation of Mohr's theory $\sigma_e = \sigma_1 - \chi\sigma_3 = \sigma_t$ [2] in this case only, which determines [3] the not quite obvious applicability range of that theory.

For an orthotropic material when its basic directions coincide with the principal directions of a stress state, if such a material has limiting stresses σ_{t1}, σ_{t2}, σ_{t3} in uniaxial tensions and σ_{c1}, σ_{c2}, σ_{c3} in uniaxial compressions in the basic and simultaneously principal directions 1, 2, 3, then the last reduction can be naturally generalized by transformation

$$\sigma_j^0 = \sigma_j/\sigma_{tj} \text{ if } \sigma_j \geq 0,\ \sigma_j^0 = \sigma_j/\sigma_{cj} \text{ if } \sigma_j \leq 0\ (j \in \{1, 2, 3, e\})$$

if necessary with renumbering the principal stresses that gives $\sigma_1^0 \geq \sigma_2^0 \geq \sigma_3^0$.

For any anisotropic material and arbitrary static loading, the last reduction can be generalized by transformation $\sigma_j^0 = \sigma_j/|\sigma_{lj}|$. Here σ_{lj} is the limiting value of a sole (uniaxial) principal stress σ_j. That value has the direction and sign of stress σ_j and acts at the same solid's point under the same other loading conditions. This is a new generalized re-comprehension of the previous reduction if σ_{tj} and σ_{cj} mean the limiting stresses in tension and compression both in the direction of the principal stress σ_j but not indispensably in the basic directions of the anisotropic material, which are not obliged to exist. All these transformations apply to any strength criteria and are universal. And, in contrast to the Tresca criterion, the universal critical state criterion

$$\sigma_e^0 = \sigma_1^0 - \sigma_3^0 = 1$$

in the reduced (relative) principal stresses σ_1^0, σ_2^0, σ_3^0 [3, 4] always conserves its simple form like all fundamental laws of nature.

References

[1] Tresca, H. E. : Memoire sur l'ecoulement des corps solides soumis a de fortes pressions. Comptes Rendus de l'Academie des Sciences, Paris, 1864, 59, 754-758

[2] Mohr, O.: Abhandlungen aus dem Gebiete der Technischen Mechanik. W. Ernst und Sohn, Berlin, 1914

[3] Gelimson, L. G.: Providing Helicopter Fatigue strength: Unit Loads. In: Structural Integrity of Advanced Aircraft and Life Extension for Current Fleets – Lessons Learned in 50 Years After the Comet Accidents, Proceedings of the 23rd ICAF Symposium, Dalle Donne, C. (Ed.), 2005, Hamburg, Vol. II, 589-600

[4] Gelimson, L. G.: Correcting and Further Generalizing Critical State Criteria in General Strength Theory. In: Review of Aeronautical Fatigue Investigations in Germany During the Period May 2005 to April 2007, (Eds.) Dalle Donne, C., Vermeer, P., CTO/IW/MS-2007-042 Technical Report, Aeronautical fatigue, ICAF2007, EADS Innovation Works Germany, 2007, 47-48

6.7 Generalization of the Huber-von-Mises-Henky Criterion in General Strength Theory

L.G. Gelimson (IFST)

For an isotropic ductile material with equal strength in tension and compression, the Huber-von-Mises-Henky criterion (of the potential energy of distortion) [1-3]

$$\sigma_e = \{[(\sigma_1 - \sigma_2)^2 + (\sigma_2 - \sigma_3)^2 + (\sigma_3 - \sigma_1)^2]/2\}^{1/2} = \sigma_l$$

(σ_1, σ_2, σ_3 the principal stresses with

$$\sigma_1 \geq \sigma_2 \geq \sigma_3,$$

σ_e the equivalent stress, and σ_l the uniaxial limiting stress) is commonly used. To generalize this criterion, divide (using ideas and approaches in similarity and dimensionality theories) each principal stress by the modulus σ_l of its ultimate value $\pm\sigma_l$ in uniaxlal state [4, 5]:

$$\sigma_1^0 = \sigma_1/\sigma_l,\ \sigma_2^0 = \sigma_2/\sigma_l,\ \sigma_3^0 = \sigma_3/\sigma_l,\ \sigma_e^0 = \sigma_e/\sigma_l.$$

The transformed criterion becomes universal:

$$\sigma_e^0 = \{[(\sigma_1^0 - \sigma_2^0)^2 + (\sigma_2^0 - \sigma_3^0)^2 + (\sigma_3^0 - \sigma_1^0)^2]/2\}^{1/2} = 1.$$

It has no evident material constant and so allows imparting a generalized sense (in comparison with this transformation) to the reduced (relative) principal stresses σ_1^0, σ_2^0, σ_3^0 according to the specific character of the strength of any given material.

For an isotropic brittle material with unequal strengths in tension and compression, reduce each principal stress by dividing it by the modulus of its ultimate value in the corresponding uniaxial state, that is σ_t in tension and $-\sigma_c$ ($\sigma_c > 0$) in compression ($j \in \{1, 2, 3, e\}$):

$$\sigma_j^0 = \sigma_j/\sigma_t \text{ if } \sigma_j \geq 0,$$

$$\sigma_j^0 = \sigma_j/\sigma_c \text{ if } \sigma_j \leq 0.$$

In this case, the universal criterion in the space of the usual principal stresses σ_1, σ_2, σ_3 is

$$\sigma_e = \{[(\sigma_1 - \sigma_2)^2 + (\sigma_2 - \sigma_3)^2 + (\sigma_3 - \sigma_1)^2]/2\}^{1/2} = \sigma_c \ (0 \geq \sigma_1 \geq \sigma_2 \geq \sigma_3);$$

$$\sigma_e = \sigma_i = \{[(\sigma_1 - \chi\sigma_2)^2 + \chi^2 (\sigma_2 - \sigma_3)^2 + (\chi\sigma_3 - \sigma_1)^2]/2\}^{1/2} = \sigma_t \ (\sigma_1 \geq 0 \geq \sigma_2 \geq \sigma_3,\ \chi = \sigma_t/\sigma_c);$$

$$\sigma_e = \{[(\sigma_1 - \sigma_2)^2 + (\sigma_2 - \chi\sigma_3)^2 + (\chi\sigma_3 - \sigma_1)^2]/2\}^{1/2} = \sigma_t \ (\sigma_1 \geq \sigma_2 \geq 0 \geq \sigma_3);$$

$$\sigma_e = \{[(\sigma_1 - \sigma_2)^2 + (\sigma_2 - \sigma_3)^2 + (\sigma_3 - \sigma_1)^2]/2\}^{1/2} = \sigma_t \ (\sigma_1 \geq \sigma_2 \geq \sigma_3 \geq 0).$$

It gives a limiting surface symmetric with respect to axis $\sigma_1 = \sigma_2 = \sigma_3$ and consisting of the two semi-infinite von Mises cylinders with radii $(2/3)^{1/2}\sigma_t$ by $\sigma_1 + \sigma_2 + \sigma_3 \geq \sigma_t$, $(2/3)^{1/2}\sigma_c$ by $\sigma_1 + \sigma_2 + \sigma_3 \leq -\sigma_c$ and of the frustum of a cone (connecting them) by $-\sigma_c \leq \sigma_1 + \sigma_2 + \sigma_3 \leq \sigma_t$.

For an orthotropic material when its basic directions coincide with the principal directions of a stress state, if such a material has limiting stresses σ_{t1}, σ_{t2}, σ_{t3} in uniaxial tensions and σ_{c1}, σ_{c2}, σ_{c3} in uniaxial compressions in the basic and simultaneously principal directions 1, 2, 3, then the last reduction can be naturally generalized by transformation ($j \in \{1, 2, 3, e\}$)

$$\sigma_j^0 = \sigma_j/\sigma_{tj} \text{ if } \sigma_j \geq 0,$$

$$\sigma_j^0 = \sigma_j/\sigma_{cj} \text{ if } \sigma_j \leq 0$$

with no renumbering σ_1 , σ_2 , σ_3 that gives $\sigma_1^0 \geq \sigma_2^0 \geq \sigma_3^0$. By

$$\sigma_{lj} = \sigma_{tj} = \sigma_{cj} \ (j = 1, 2, 3),$$

we obtain the Hu-Marin criterion (as a particular case) but with σ_e^0

$$\sigma_e^0 = [\sigma_1^2/(\sigma_{l1})^2 + \sigma_2^2/(\sigma_{l2})^2 + \sigma_3^2/(\sigma_{l3})^2 - \sigma_1\sigma_2/(\sigma_{l1}\sigma_{l2}) - \sigma_2\sigma_3/(\sigma_{l2}\sigma_{l3}) - \sigma_3\sigma_1/(\sigma_{l3}\sigma_{l1})]^{1/2} = 1$$

and (by $\sigma_{tj} \neq \sigma_{cj}$ in some direction j) its generalization, e.g., by $\sigma_1 \geq 0$, $\sigma_2 \leq 0$, $\sigma_3 \leq 0$,

$$\sigma_e^0 = [\sigma_1^2/(\sigma_{t1})^2 + \sigma_2^2/(\sigma_{c2})^2 + \sigma_3^2/(\sigma_{c3})^2 - \sigma_1\sigma_2/(\sigma_{t1}\sigma_{c2}) - \sigma_2\sigma_3/(\sigma_{c2}\sigma_{c3}) - \sigma_3\sigma_1/(\sigma_{c3}\sigma_{t1})]^{1/2} = 1.$$

For any anisotropic material and arbitrary static loading, the last reduction is also generalized:

$$\sigma_j^0 = \sigma_j/|\sigma_{lj}|.$$

By this transformation, σ_{lj} is the limiting value of a sole (uniaxial) principal stress σ_j. That value has the direction and sign of σ_j and acts at the same solid's point under the same other loading conditions. This is a new generalized re-comprehension of the previous reduction if σ_{tj} and σ_{cj} mean the limiting stresses in tension and compression both in the direction of σ_j but not indispensably in the basic directions of the anisotropic material which are not obliged to exist. All these universal transformations apply to any strength criteria. And, in contrast to the Huber-von-Mises-Henky criterion, the universal critical state criterion in σ_1^0, σ_2^0, σ_3^0 [4, 5] always conserved its simple form like all fundamental laws of nature.

References

[1] Huber, M. T.: Die spezifische Formänderungsarbeit als Maß der Anstrengung eines Materials. Czasopismo Techniczne, Lemberg (Lwow), 1904

[2] von Mises, R.: Mechanik der festen Körper im plastisch-deformablen Zustand. Nachrichten der Gesellschaft der Wissenschaften, Göttingen, 1913

[3] Henky, H.: Zur Theorie plastischer Deformationen. Zeitschrift angewandter Mathematik und Mechanik, 1924

[4] Gelimson, L. G.: Elastic Mathematics. General Strength Theory. The "Collegium" All World Academy of Sciences Publishers, Munich, 2004

[5] Gelimson, L. G.: Providing Helicopter Fatigue strength: Unit Loads. In: Structural Integrity of Advanced Aircraft and Life Extension for Current Fleets – Lessons Learned in 50 Years After the Comet Accidents, Proceedings of the 23rd ICAF Symposium, Dalle Donne, C. (Ed.), 2005, Hamburg, Vol. II, 589-600

7 Fatigue and Fracture of Engine Materials

7.1 Fatigue Strength Reduction of TiAl-Alloys by Impact Damage

S. Gebhard (DLR), J. Hausmann (DLR), P. Peters (DLR), D. Roth-Fagaraseanu (RR), F. Turley (RR) and H. Voggenreiter (DLR)

The inherent low damage tolerance of gamma-based TiAl-alloys is one of the main reasons currently limiting their application in gas turbines. Therefore, the impact behaviour of the promising alloy TNBV3B produced by three different processing routes –cast, forged (with a small degree of deformation) and extruded- has been studied making use of ballistic tests. The damage evolution due to centre and edge impacts on flat and airfoil-like shaped specimens has been investigated. Geometrical effects as well as the influence of the microstructure were studied.
Fatigue experiments at room temperature and 400 °C were performed to determine the threshold for crack growth as a function of the edge damage size. For these tests, specimens showing cracks with lengths up to some millimeters on the specimen back side as well as specimens with blow-outs were chosen. For long cracks (in relation to the indent diameter) the fatigue strength depends on the damage extension (crack length, K_{th}-controlled). In case of low energy impacts causing small cracks (≈ size of the indent diameter) the micro-damage as well as the deformation hardened zone can exert an important influence on the damage development during fatigue.

The area deformed by the impact was characterized with the help of hardness measurements on sectioned specimens. From a correlation between hardness and plastic (compressive) deformation determined by performing micro-hardness tests on compressively (up to 15%) deformed specimens, the degree of deformation caused by the impact was determined.

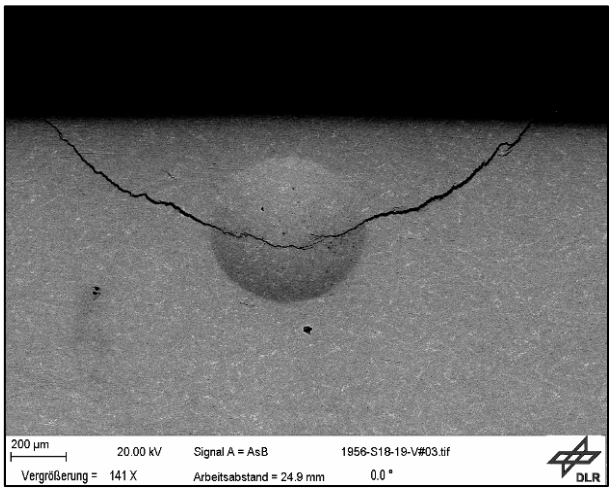

Figure 7.1 Front side damage of an edge impacted specimen before fatigue testing.

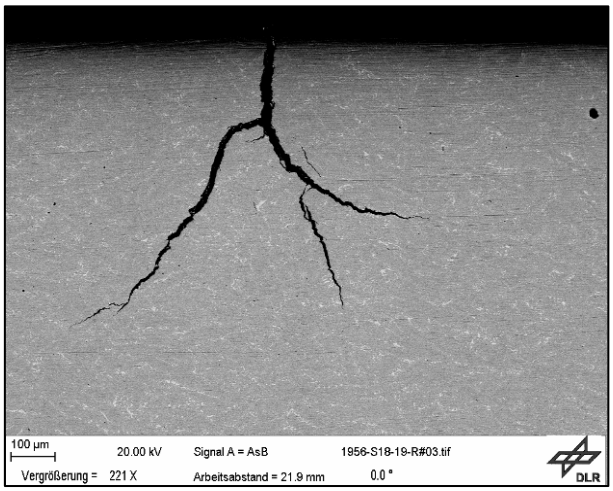

Figure 7.2 Back side crack network of the same edge impacted specimen before fatigue testing.

8 Non-Destructive Testing and Structural Health Monitoring

8.1 Influence of Cyclic Loading and Temperature on Integrity of Piezoceramic Patch Transducers

M. Gall and B. Thielicke (Fraunhofer)

The loading limits, damage behaviour and long-term integrity of piezo-ceramic patch transducers, based on monolithic PZT wafers [1], were studied. Based on the electro-mechanical coupling properties of piezo-ceramics in actuator and/ or sensor-applications, these transducers show high potential for aeronautical applications in non-destructive testing and structural health monitoring as well as vibration and noise control issues. The laminar, composite design of the patches allows for direct application to flat or curved surfaces or even integration into fibre composite materials, making them especially attractive for applications in light-weight constructions. Under working conditions the patches have to withstand the operational demands to which the main structure is subjected, above all the basic mechanical loading and environmental conditions as well as electrical actuation loading. The electro-mechanical loading history can eventually lead to degradation of the mechanical and electrical properties or even to complete failure of the device. The overall goal of the study is to provide potential users of the patches with the needed information on expected performance and life-span under given application-specific loading conditions.

Experimental & Numerical Work and Results
For testing, the patches were glued onto the middle section of CFRP-substrate sheets, and loaded in a 4-point bending test setup such that the piezo-ceramic wafer was subjected to nearly constant axial strains [2] (see Figure 8.1). This setup allows quasi-static and cyclic loading of the patches under mechanical tensile or compressive strain, while simultaneously testing the patch-to-structure bond under working conditions. To monitor the sensor performance of the patches during testing, the electric sensor signal of the patches was evaluated and the patches were visually inspected for integrity.

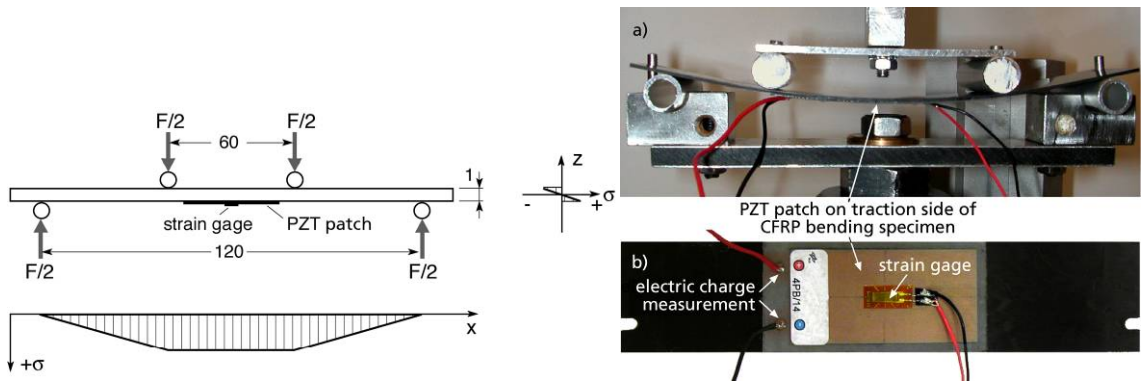

Figure 8.1 Loading principle and setup of 4-point-bending test (here: a) PZT patch under tensile loading, b) patch on CRFP specimen).

The strain-cycle fatigue life diagram of the investigated wafer-based PZT patches for tensile loading at RT was successfully extended to cover a temperature range from -40° C to +100 °C. At all investigated temperatures, cracking of the PZT wafer was identified as the relevant damage mechanism, causing significant degradation of the sensor performance (failure criterion: below 90 % of initial value). At RT the average loading limit which caused in-

stantaneous failure was determined at 0.35 % tensile strain. At elevated temperatures the loading limits as well as the sustainable cyclic strain level were found to be reduced. At -40 °C all testing results were very close to RT data.

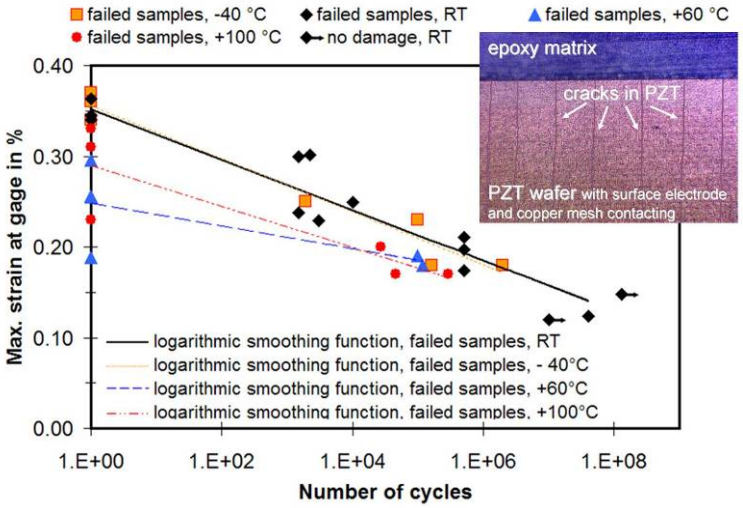

Figure 8.2 Fatigue life diagram for mechanical tensile loading of PZT patches at different temperatures. Insertion: typical damage pattern (cracks in PZT).

Under compressive loading, up to -0.6 % strain could be sustained by the patches without any mechanical damage.
The performance of the patches under electric activation was studied in a bending actuator test as well as on patches applied to massive glass substrate (nearly rigid clamping). Under the maximum bipolar electric field of -500 … +2000 V/mm, all samples survived at least 10^8 cycles.

Numerical simulation showed good agreement between the experimental data and simulation results and proved to be a practical tool to interpret experimental findings. Based on microstructural investigations of the cracked PZT wafers and FE-simulation, fracture mechanics analyses of the local stress situation in the PZT ceramic were carried out and showed good predictability of the RT loading limits, in correlation to initial defect sizes. Also, a good predictability of attainable effects for piezoelectric actuators/ sensors in smart structures can be achieved by simulation [3, 4].

Acknowledgments
Financial support by the German Research Society DFG in the program “Adaptronics in Machine Tools” is gratefully acknowledged.

References

[1] P. Wierach, H.P. Monner, A. Schönecker and J.K. Dürr, 2002, “Application Specific Design of Adaptive Structures with Piezoceramic Patch Actuators,” proc. of SPIE 4698, pp. 333-341.
[2] B. Thielicke, T. Gesang and P. Wierach, 2003, “Reliability of piezoceramic patch sensors under cyclic mechanical loading,” Smart Mater. Struct., 12 (6), pp. 993-996.
[3] M. Gall and B. Thielicke, 2007, “Life-span investigations of piezoceramic patch sensors and actuators,” proc. of SPIE, 6526, pp. 65260P.
[4] M. Gall and B. Thielicke, 2008, Influence of Cyclic Loading and Temperature on Integrity of Piezoceramic Patch Transducers, Proc. of SMASIS08, ASME Conference on Smart Materials, Adaptive Structures and Intelligent Systems, October 28-30, 2008, Ellicott City, MD, USA, ISBN 978-0-7918-3839-6, paper 341.

8.2 Corrections and Generalizations of the Least Square Method

L.G. Gelimson (IFST)

For any data processing, the least square method [1] by Legendre and Gauss is practically the unique known one applicable to contradictory problems. But this method is based on the absolute error not invariant by equivalent transformations of a problem and ignores the possibly noncoinciding physical dimensions (units) of relations in a problem. The method does not correlate the deviations of the desired approximation from the approximated objects with these objects themselves and simply mixes those deviations without their adequate weighing. The method considers equal changes of the squares of those deviations with relatively less and greater moduli (absolute values) as equivalent ones. It foresees no iterating, is based on a fixed algorithm accepting no a priori flexibility, and provides no own a posteriori adapting. These defects in the essence of the least square method result in many fundamental shortcomings in its applicability. The method loses any sense and is not applicable at all to problems simulated by a set of equations with different physical dimensions (units), e.g., to a mechanics problem with one equation via the impulse conservation law and another equation via the energy conservation law. There is no result invariance by equivalent transformations of a problem and no objective sense of the result along with possibly ignoring some part of a problem and paradoxical approximation. And the method presents each result as the highest truth without any justification.

For extending the least square method via setting a general problem, let $Z \subseteq X \times Y$ be a point set to be approximated by a function (curve) in $X \times Y$ with an expansion $y = \sum_{k=0}^{m} a_k f_k(x)$. Here $x \in X$, $y \in Y$, $a_k \in R$, $m \in N = \{0, 1, 2, ...\}$ with using certain given "standard" functions $f_k(x)$ defined on X with ranges in Y and taken with any real factors (coefficients) to be chosen. The problem consists in finding (in this class) functions with graphs nearest to Z in a certain reasonable sense. To exactly fit this, $Z \subseteq \{ (x, y) \mid x \in X \}$ should hold. Otherwise,

$$^2S = \sum_{x \in Z/X} R_x (r_x (\sum_{k=0}^{m} a_k f_k(x), y)), \; ^2S = \sum_{x \in Z/X} r^2(\sum_{k=0}^{m} a_k f_k(x), y)$$

where R_x and r_x (which can be similar to distances in $Y \times Y$) are some nonnegative functions generally individual for different $x \in Z/X$; R and r are (independently from x) the second power function and the distance, respectively. ^2S has to be minimized as a measure of nearness. Let Z/X be a finite point set

$$\{_{i=0}^{n} (x_i, y_i) \} = \{ (x_0, y_0), (x_1, y_1), (x_2, y_2), ... , (x_n, y_n) \}.$$

To provide belonging all the n +1 points to the above graph, the set of n +1 equations

$$\sum_{k=0}^{m} a_k f_k(x_i) = a_0 f_0(x_i) + a_1 f_1(x_i) + a_2 f_2(x_i) + ... + a_m f_m(x_i) = y_i , \; i \in \{0, 1, 2, ... , n\}$$

with m +1 unknown factors (coefficients) $a_0 , a_1 , a_2 , ... , a_m$ to be found, has to hold. Keeping X arbitrary, consider Y multidimensional and receive the set of m +1 linear equations

$$Y \subseteq R^p, \; y_i = (y_i^{(1)}, y_i^{(2)}, ... , y_i^{(p)}), \; f_k(x_i) = (f_k^{(1)}(x_i), f_k^{(2)}(x_i), ... , f_k^{(p)}(x_i)), \; p \in N^+ = \{1, 2, ... \},$$

$$\sum_{k=0}^{m} a_k \sum_{i=0}^{n} \sum_{l=1}^{p} f_k^{(l)}(x_i) f_s^{(l)}(x_i) = \sum_{i=0}^{n} \sum_{l=1}^{p} f_s^{(l)}(x_i) y_i^{(l)} , \; s \in \{0, 1, 2, ... , m\}.$$

By the proposed iteration method of the least normed powers [2], instead of absolute errors, autoerrors are minimized, and both the power and the autoerror parameters may be freely chosen. The known formulae in the least square method can be used also here by m = 2 to determine all the currently unknown variables in the next approximation in the numerators after replacing all the variables in the prior approximation with their values already known in the denominators. Replacing the autoerrors with the reserves that naturally have to be maximized brings a further method generalization also applicable to determining the supersolution [2] to a set of relations.

By an autoerror equalizing iteration method [2], order the quantiset of the autoerrors $\delta_\lambda^{(k)}$ of each (λth) equation ($\lambda \in \Lambda$). The left-hand sides of two equations with the greatest absolute value of

the difference of their autoerrors $\delta_\lambda^{(k)}$ with corresponding indexes λ are setting equal to each other. Repeat this for the remaining equations, and so on. By every step of designing such an equalizing quantiset of equations, each initial equation is used at most once if possible. If this quantiset contains all the possible independent new equations and nevertheless has more than one solution, the required amount of additional new equations that express equalizing the greatest autoerrors $\delta_\lambda^{(k)}$ to zero must be also designed. Stabilizing the equalizing quantiset, its quasisolution approximation, and the autoerrors of the separate initial equations and of their quantiset can be a criterion for finishing the iterations.
A direct-solution method [2] proposes the approximation (Q the multiquantity)

$$x = Q(A')//Q(A)(... + \alpha a/||a||^n + ... + \beta b/||b||^n + \ldots)//(\ldots + \alpha/||a||^n + \ldots + \beta/||b||^n + \ldots)$$

to any quantiset A using also A' after excluding exactly all quantielements with zero elements:

$$A = \{... , {}_\alpha a, ... , {}_\beta b, ... , {}_\gamma 0, ...\}^\circ, \quad A' = \{... , {}_\alpha a, ... , {}_\beta b, ... \}^\circ$$

whose elements ... , a, ... , b, ... , 0, ... belong to a common normed vector space and their quantities ... , α, ... , β, ... , γ, ... are nonnegative real numbers.
These methods are very effective by solving problems simulated by overdetermined quantisets of equations, which is always the case by best approximating experimental data.

[1] Encyclopaedia of Mathematics. Ed. M. Hazewinkel. Volumes 1 to 10. Kluwer Academic Publishers, Dordrecht, 1988-1994
[2] Gelimson, L. G.: Elastic Mathematics. General Strength Theory. The "Collegium" All World Academy of Sciences Publishers, Munich, 2004

8.3 General Theory of Measuring Inhomogeneous Distributions

L.G. Gelimson (IFST)

Measuring a physical magnitude not uniformly distributed in space and/or time [1] by means of a real physical device with nonzero sizes and inertia leads to inadequate measurement data. They are distorted (modulated) by some law and differ from the true distributions. The known measurement ways based on inadequate design methods cannot define the true distributions.
The purpose of the present theory is to reliably define the true distributions of inhomogeneous magnitudes. This is achieved by designing and applying adequately modeling measurement processes. The distinctive feature of the proposed theory of measuring inhomogeneous distributions is using new calculation formulae to determine the true distributions.
Let a one-variable function $p(s)$ be continuously distributed and integral-mean modulated on each segment of a constant length Δ. Then the measurement operator to be inverted is [2-4]

$$M_\Delta: p(s) \to \underline{p}(s) = \Delta^{-1}\int_{s-\Delta/2}^{s+\Delta/2} p(t)dt.$$

The domain of $p(s)$ can be restricted by not greater than Δ from each boundary point. If $p(s)$ and $q(s)$ are solutions to this equation,

$$r(s) = q(s) - p(s)$$

is a solution to the equation [2-4]

$$\int_{s-\Delta/2}^{s+\Delta/2} r(t)dt = 0.$$

Its differentiating by s shows that for each s from the domain of definition, the equality

$$r(s + \Delta/2) = r(s - \Delta/2)$$

is an identity. Therefore, $r(s)$ is a periodic function with period Δ. The integral mean value of this function on each segment of length Δ vanishes. The inversion of M_Δ is therefore ambiguous and

determined up to such a function $r(s)$, e.g., a finite or infinite sum of harmonic functions with divisors of Δ as periods. Let the device be such a suitable one that the variation of the distribution $p(s)$ on each segment of length Δ is small enough in comparison with the least value of the distribution itself on the same segment. Then such a function $r(s)$ can be considered vanishing and the inversion practically unambiguous. Otherwise, it is necessary and sufficient to additionally use another device with such constant Δ' that Δ'/Δ is theoretically irrational and practically an uncancellable fraction with a sufficiently great sum of the numerator and denominator. If there is a continuous inversion of M_Δ, then the function $\underline{p}(s)$ is continuously differentiable, and vice versa. By known discrete values of $\underline{p}(s)$ with measurement errors, interpolation and numerical differentiation lead to great errors. It is better to *a priori* choose standard functions whose linear combinations can be considered proper. When *a priori* choosing the coefficients by the arguments of those functions, due to the linearity of the measurement operator, we receive linear equations with unknown factors in the combinations, whose set is usually overdetermined and thus contradictory. The methods proposed by the author are very suitable for it and quickly lead to its quasisolutions. What is more, this brings no increasing but correcting measurement errors.

By many most important standard functions, using the measurement operator can be replaced with multiplication by a suitable factor. For example, this factor is 1 for each linear function,

$$\mathrm{sh}(0.5n\Delta)/(0.5n\Delta) \text{ for } \exp(ns), \mathrm{sh}\, ns, \text{ and } \mathrm{ch}\, ns;$$

$$\sin(0.5n\Delta)/(0.5n\Delta) \text{ for } \sin ns \text{ and } \cos ns.$$

By a continuous function $p(s)$ with period 2π, due to the uniform summability and hence integrability of the Fourier series, we have [2-4]

$$p(s) = 0.5c_0 + \sum_{n=1}^{\infty} (c_n \cos ns + s_n \sin ns),$$

$$\underline{p}(s) = 0.5c_0 + \sum_{n=1}^{\infty} [\sin(0.5n\Delta)/(0.5n\Delta)](c_n \cos ns + s_n \sin ns).$$

The inversion algorithm is hence determining the factors of $\underline{p}(s)$ and then the factors of $p(s)$:

$$\underline{p}(s) = 0.5\underline{c}_0 + \sum_{n=1}^{\infty} (\underline{c}_n \cos ns + \underline{s}_n \sin ns),$$

$$p(s) = 0.5\underline{c}_0 + \sum_{n=1}^{\infty} [0.5n\Delta/\sin(0.5n\Delta)](\underline{c}_n \cos ns + \underline{s}_n \sin ns).$$

General theory of measuring inhomogeneous distributions applies to any problem in measurement technology and is especially useful and even urgent by very heterogeneous objects and rapidly changeable processes. A delay usually stable is simply compensated by a corresponding displacement of the measurement data in the positive direction of the time axis.

[1] Handbuch Struktur-Berechnung. Prof. Dr.-Ing. L. Schwarmann. Industrie-Ausschuss-Struktur-Berechnungsunterlagen, Bremen, 1998

[2] Gelimson, L. G.: Elastic Mathematics. General Strength Theory. The “Collegium” All World Academy of Sciences Publishers, Munich, 2004

[3] Gelimson, L. G.: Providing Helicopter Fatigue strength: Unit Loads. In: Structural Integrity of Advanced Aircraft and Life Extension for Current Fleets – Lessons Learned in 50 Years After the Comet Accidents, Proceedings of the 23rd ICAF Symposium, Dalle Donne, C. (Ed.), 2005, Hamburg, Vol. II, 589-600

[4] Gelimson, L. G.: Theory of Measuring Stress Concentration. In: Review of Aeronautical Fatigue Investigations in Germany During the Period May 2005 to April 2007, (Eds.) Dalle Donne, C., Vermeer, P., CTO/IW/MS-2007-042 Technical Report, Aeronautical fatigue, ICAF2007, EADS Innovation Works Germany, 2007, 53-54